



A T cell receptor targeting a recurrent driver mutation in FLT3 mediates elimination of primary human acute myeloid leukemia *in vivo*

Received: 16 November 2022

Accepted: 28 August 2023

Published online: 02 October 2023

Check for updates

Eirini Giannakopoulou^{1,2}, Madeleine Lehander³, Stina Virding Culleton³, Weiwen Yang^{1,2}, Yingqian Li^{1,2}, Terhi Karpanen^{1,2,4}, Tetsuichi Yoshizato³, Even H. Rustad^{1,2}, Morten Milek Nielsen^{1,2}, Ravi Chand Bollineni^{1,2}, Trung T. Tran⁵, Marina Delic-Sarac^{1,2}, Thea Johanne Gjerdingen^{1,2}, Karolos Douvlataniotis^{1,2}, Maarja Laos^{1,2}, Muhammad Ali^{1,2}, Amy Hillen^{1,2}, Stefania Mazzi³, Desmond Wai Loon Chin³, Adi Mehta⁷, Jeppe Sejerø Holm⁸, Amalie Kai Bentzen⁸, Marie Bill⁹, Marieke Griffioen¹⁰, Tobias Gedde-Dahl¹¹, Sören Lehmann^{3,12,13}, Sten Eirik W. Jacobsen^{1,2,14,15}✉, Petter S. Woll^{1,2,15}✉ & Johanna Olweus^{1,2}✉

Acute myeloid leukemia (AML), the most frequent leukemia in adults, is driven by recurrent somatically acquired genetic lesions in a restricted number of genes. Treatment with tyrosine kinase inhibitors has demonstrated that targeting of prevalent FMS-related receptor tyrosine kinase 3 (FLT3) gain-of-function mutations can provide significant survival benefits for patients, although the efficacy of FLT3 inhibitors in eliminating FLT3-mutated clones is variable. We identified a T cell receptor (TCR) reactive to the recurrent D835Y driver mutation in the FLT3 tyrosine kinase domain (TCR^{FLT3D/Y}). TCR^{FLT3D/Y}-redirected T cells selectively eliminated primary human AML cells harboring the FLT3^{D835Y} mutation *in vitro* and *in vivo*. TCR^{FLT3D/Y} cells rejected both CD34⁺ and CD34⁻ AML in mice engrafted with primary leukemia from patients, reaching minimal residual disease-negative levels, and eliminated primary CD34⁺ AML leukemia-propagating cells *in vivo*. Thus, T cells targeting a single shared mutation can provide efficient immunotherapy toward selective elimination of clonally involved primary AML cells *in vivo*.

Neoantigens represent an attractive group of targets in cancer immunotherapy, as they are tumor specific and can be recognized by T cells as foreign in the context of major histocompatibility complex (MHC)^{1–4}. Neoantigenic burden is an important determinant of clinical success upon checkpoint inhibition^{5–7}, and case reports have demonstrated that neoantigen-reactive T cells can mediate clinical responses^{8–10}.

This has brought hope that T cells genetically modified to express TCRs derived from neoantigen-reactive T cells could provide efficient adoptive cell therapy. Patient T cells do, however, spontaneously recognize only 1–2% of candidate neoantigens predicted to be expressed and presented on human leukocyte antigen (HLA) in solid cancer¹¹. As the large majority is unique to the individual patient, therapeutic

targeting of neoantigens generally becomes a highly personalized effort¹². In addition to being resource demanding, such a strategy might not benefit patients in time. By contrast, public neoantigens derived from recurrent oncogenic mutations have the advantage that a single TCR with off-the-shelf availability could target larger patient groups. Although shared mutations resulting in neoantigens presented on frequently expressed HLA alleles are rare in solid cancer, promising results were recently shown with T cells engineered to express a TCR targeting mutant KRAS in a patient with pancreatic adenocarcinoma¹³ and mutant p53 in a patient with breast cancer¹⁴.

AML is, in contrast to solid tumors, characterized by recurrent driver mutations in a restricted number of genes¹⁵, many of which are screened for in routine diagnostics. The only curative therapeutic option for many patients with AML today is allogeneic hematopoietic stem cell transplantation (allo-HSCT). Allo-HSCT remains, however, associated with high relapse rates as well as transplant-related morbidity and mortality resulting from donor T cells attacking healthy recipient cells, causing severe graft-versus-host disease¹⁶, and often a suitable donor cannot be identified. This has prompted development of alternative cellular therapies^{17,18}. Successful targeting of the lymphoid-specific molecule CD19 in chimeric antigen receptor (CAR) T cell therapy of acute lymphocytic leukemia, has led to attempts at also directing CARs to myeloid cell surface antigens, including CD33 (ref. 19), CD123 (ref. 20) and FLT3 (ref. 21), overexpressed on AML cells. However, these molecules are also highly expressed on normal myeloid progenitor cells and even on hematopoietic stem cells, representing a major challenge^{22–24}. Thus, CAR T cell therapies targeting these molecules are associated with toxicities and a need for transplantation to rescue normal hematopoiesis after a short period of treatment (for example, NCT03126864) (ref. 25). It is also unclear whether all AML-propagating cells express these antigens and therefore whether targeting has curative potential²⁶.

Cytotoxic cells modified to express TCRs provide an opportunity to also target intracellular antigens with restricted expression in normal tissues, such as the specialized DNA polymerase terminal deoxynucleotidyl transferase (TdT)²⁷, dramatically broadening the repertoire of potential targets. To this end, TCRs recognizing Wilms tumor 1 (WT1) were recently shown to reduce relapses in patients with AML after transplantation²⁸. A TCR recognizing the recurrent neoantigen nucleophosmine 1 (NPM1) presented on HLA-A*02:01 (ref. 29,30) and T cell clones targeting the fusion core-binding factor subunit β (CBFB)-myosin heavy chain 11 (MYH11) in the context of HLA-B*40:01 (ref. 31) showed some efficacy in patient-derived xenograft (PDX) mouse models with low AML engraftment. However, no neoantigen-specific TCR has yet been shown to efficiently target primary human AML in *in vivo* models in which high and increasing leukemic burden is observed.

Recurrent driver mutations in *FLT3* occur in approximately one-third of patients with de novo AML as internal tandem duplications (ITD) in the juxtamembrane domain or point mutations in the activation loop of the tyrosine kinase domain (Fig. 1a), which are screened for in routine diagnostics of AML³². Although, in most cases, *FLT3* mutations are secondary events in leukemogenesis³³, they are associated with accelerated clonal expansion and disease progression, and treatment with the tyrosine kinase inhibitor (TKI) midostaurin in patients with *FLT3* mutations receiving standard induction chemotherapy does significantly increase long-term survival³⁴. This indicates that *FLT3*-mutated AML clones have a survival advantage during standard therapy, expanding to drive relapse unless effectively eradicated, but the efficacy of TKIs in eliminating *FLT3*-mutated clones remains variable^{35–37}.

Because of varying length, ITDs do not encode shared neoantigens. Mutations in the D835 position of *FLT3* represent the most frequent point mutations in *FLT3* (7–10% of patients with AML), with aspartic acid (D) to tyrosine (Y) being by far the most common amino acid substitution, although other substitutions can also occur³². The effect of TKIs on the D835Y mutation (*FLT3*^{D835Y}) is limited by this mutation conferring primary and secondary resistance to first- and second-generation type II TKIs^{35–37}.

We recently demonstrated that healthy donor T cells provide a rich source of neoantigen-reactive TCRs^{38,39}. Here, we used this technology to identify a TCR reactive to a peptide from *FLT3*^{D835Y}. The TCR (TCR^{FLT3D/Y}) is restricted by HLA-A*02:01 (hereafter HLA-A2), expressed in approximately 50% of people of European, Middle Eastern or North African ancestry. We demonstrate that T cells redirected with TCR^{FLT3D/Y} (TCR^{FLT3D/Y} cells) specifically and efficiently eliminate primary human AML cells harboring *FLT3*^{D835Y} *in vitro* and *in vivo*, while sparing cells expressing wild-type (WT) *FLT3*.

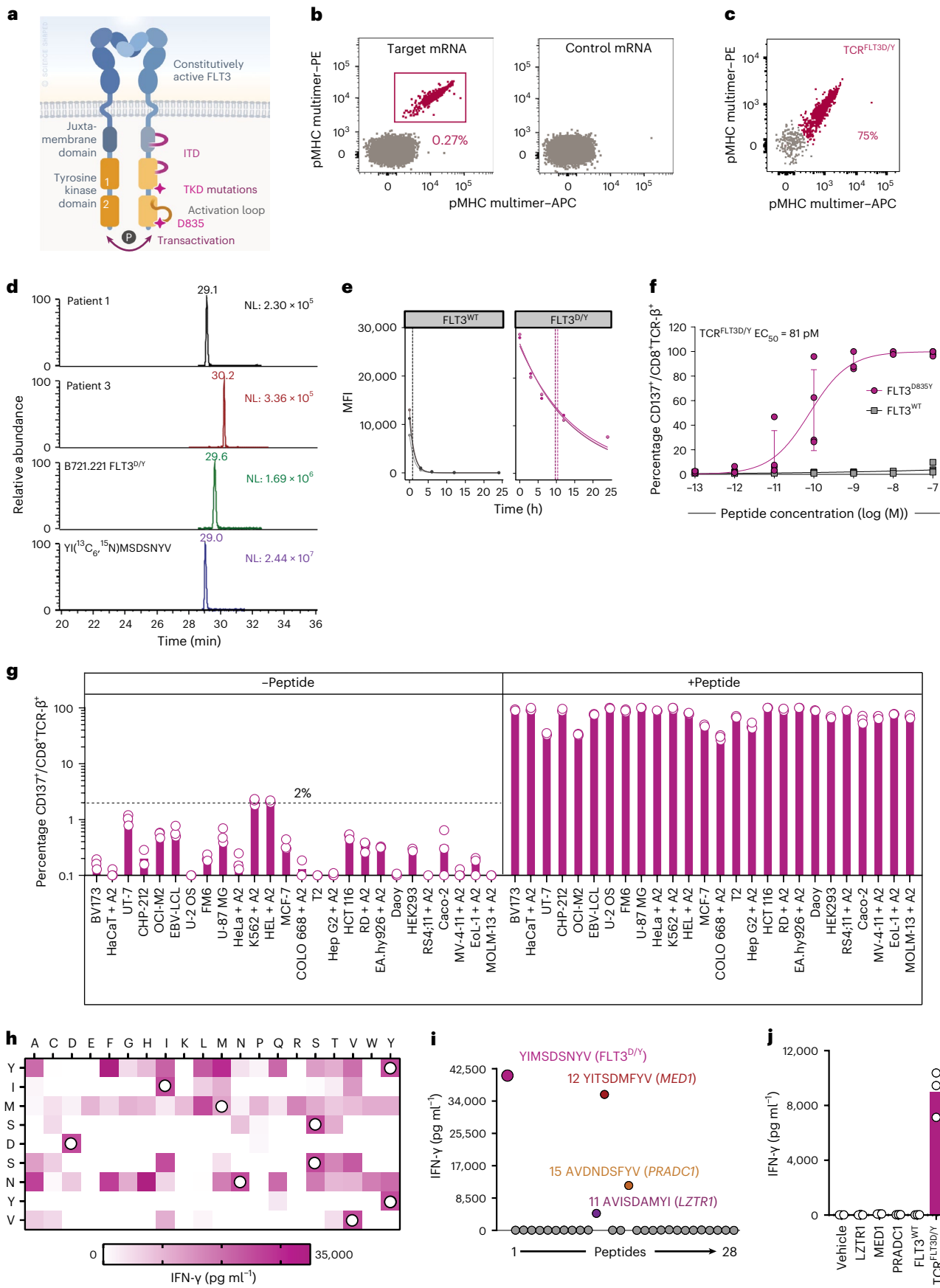
Results

Inducing *FLT3*^{D835Y}-reactive T cells from healthy donor T cells

Naive T cells from a large number of HLA-A2-positive healthy blood donors ($n = 16$) were co-cultured with autologous monocyte-derived dendritic cells (moDCs) electroporated with mRNA encoding a 9-mer and a 10-mer peptide with the *FLT3*^{D835Y} mutation in position 1, predicted to be strong binders to HLA-A2 (Extended Data Fig. 1a). The sequence was flanked by 9–11 amino acids at the N-terminal and C-terminal end (target mRNA, encoding KICDFGLARYIMSDSNVVRGNVLARLP) or control mRNA. After 10 d of co-culture, cells were stained with dual-color peptide–MHC (pMHC) multimers complexed with the nonameric or decameric peptide in which the *FLT3*^{D/Y} mutation was in position 1. Multimer^{*}CD8⁺T cells reactive with the 9-mer were detected in only one donor and only in the culture primed with the target mRNA

Fig. 1 | TCR^{FLT3D/Y} cells specifically recognize mutated peptide with high sensitivity in an HLA-A2-restricted manner and do not show off-target reactivity. **a**, Schematic illustration of *FLT3*. TKD, tyrosine kinase domain. **b**, Naive CD8⁺ T cells co-cultured with autologous HLA-A2⁺ mRNA-transfected moDCs stained with *FLT3*^{D/Y} pMHC multimers. **c**, CD8⁺ T cells transduced to express TCR^{FLT3D/Y} stained with *FLT3*^{D/Y} pMHC multimers (Gating strategy in Extended Data Fig. 3b). **d**, Parallel reaction-monitoring analysis, targeting the *FLT3*^{D835Y} peptide ($m/z = 1,091,4389^{1+}$) in primary AML cells from two patient samples and the B721.221 cell line transduced to express *FLT3*^{D835Y} and HLA-A2. NL = normalization level. **e**, Off-rates for *FLT3*^{WT} or *FLT3*^{D/Y} peptide binding to HLA-A2 measured by flow cytometry. Vertical lines indicate calculated half-lives in each experiment. Dots represent mean fluorescence intensity (MFI) values of intact pMHC complexes on fluorescent particles at the indicated time points (h) (one replicate per experiment, $n = 3$ independent experiments). **f**, Activation of TCR^{FLT3D/Y} cells (CD137⁺) co-incubated with peptide-pulsed K562 cells. Data points are from $n = 4$ donors transduced to express TCR in $n = 3$ independent experiments, with each circle representing the mean of three technical replicates per donor, shown as mean \pm s.e.m. **g**, Activation of CD8⁺ TCR^{FLT3D/Y} cells co-incubated with HLA-A2⁺ cell lines with or without *FLT3*^{D/Y} peptide. Results are

from one experiment representative of $n = 4$ (BVI73, CHP-212, EBV-LCL, K562, Daoy, RS4;11), $n = 3$ (HaCaT, U-2 OS, FM6, U-87 MG, HeLa, MV-4-11, EoL-1, MOLM-13) or, for the remaining cell lines, $n = 2$ independent experiments using different T cell donors; data points represent $n = 3$ technical replicates. The suffix + A2 denotes that cell lines were transduced with HLA-A*02:01, whereas remaining cell lines naturally express it. Connecting lines in **f** and bars in **g** show mean. The dashed line in **g** shows the highest level of activation by cell lines alone. **h–j**, IFN-γ produced by TCR^{FLT3D/Y} cells co-incubated with K562 cells loaded with peptides from the mimotope library (**h**) or pulsed with the peptides that were predicted as potentially cross-reactive from the *in silico* search (**i**) or transfected with mRNA constructs encoding 30–32-mer peptides with the candidate cross-reactive peptide inducing reactivity (shown in **i**) in the middle, flanked by its naturally occurring sequence, or transfected with mRNA encoding the *FLT3*^{D/Y} epitope or *FLT3*^{WT} (**j**). White circles in **h**, amino acids of the *FLT3*^{D/Y} peptide. Positive reaction for IFN-γ, 5,000–35,000 pg ml⁻¹. LZTR1, leucine zipper-like post-translational regulator 1; MED1, mediator complex subunit 1; PRADCI, protease-associated domain-containing protein 1. Data in **h–j** are from one of $n = 2$ independent experiments, and individual data points represent one (**h,i**) or three (**j**) technical replicates.



and were sorted. Only one functional TCR sequence (TCR^{FLT3D/Y}) was identified from two clones and from 55 sorted, sequenced single cells (Fig. 1b and Extended Data Fig. 1b,c).

By contrast, memory cytotoxic T lymphocytes reactive to FLT3^{D835Y} HLA-A2 were not identified among peripheral blood (PB) mononuclear cells (PBMCs) from diagnostic AML samples ($n=3$) or from samples after allo-HSCT with HLA-matched donors ($n=3$), directly after thawing or following a short 5-d in vitro culture in the presence of 100 nM of the FLT3^{D/Y} mutant peptide to expand memory T cells (Extended Data Fig. 1d,e).

TCR^{FLT3D/Y} recognizes mutant peptide with high peptide–HLA stability

The TCR^{FLT3D/Y} sequence was efficiently expressed in third-party PB T cells by retroviral transduction (Fig. 1c). Binding to HLA-A2 as well as endogenous processing and presentation of the peptide was demonstrated by immunopeptidomics and targeted mass spectrometry analysis of primary AML cells from two patients, using a monoallelic cell line overexpressing the FLT3^{D835Y} mutation as a positive control (Fig. 1d, with ion chromatograms extracted using the precursor → b2, b3, b4, b5, b6, b7 and b8 fragment ion transactions, and Extended Data Fig. 2). We previously demonstrated that peptide–HLA stability is strongly predictive of neoantigen immunogenicity³⁸, and the complex of HLA-A2 and the mutated peptide had an almost tenfold longer half-life than that of the WT peptide complexed with HLA-A2 (mean of 9.9 versus 0.83 h, $n=3$) (Fig. 1e). In agreement with this, TCR^{FLT3D/Y} cells stained brightly with pMHC multimers presenting mutant, but not WT, peptide (Extended Data Fig. 3a). A similar fraction of TCR^{FLT3D/Y}-redirected CD8⁺ T cells stained positively with FLT3^{D/Y} pMHC multimers and anti-mouse TCR-β-PE (reactive to the mouse constant region introduced into the TCR⁴⁰) and negatively with anti-human TCR-α, indicating preferential pairing of the introduced TCR-α and TCR-β chains and suppression of the endogenous TCR (Extended Data Fig. 3b,c). Both CD8⁺ and CD4⁺ T cells exhibited a predominantly naive profile and expanded similarly to T cells transduced to express a control TCR in vitro, the clinically applied NY-ESO1-specific 1G4 (TCR^{1G4}) (ref. 41), indicating lack of fratricide (Extended Data Fig. 3d,e).

TCR^{FLT3D/Y} cells show high peptide sensitivity and specificity

TCR^{FLT3D/Y} cells recognized K562 target cells transduced to express HLA-A2 and pulsed with picomolar concentrations of the mutant peptide (half-maximal effective concentration (EC_{50}) = 81 pM) and displayed no reactivity against the corresponding WT peptide (Fig. 1f). By comparison, TCR^{1G4} cells recognized the cognate NY-ESO1 peptide with an EC_{50} of 5.5 nM (Extended Data Fig. 3f), in agreement with previous data showing an EC_{50} of 7.7 nM⁴². Furthermore, TCR^{FLT3D/Y} cells showed no or negligible reactivity to a panel of 26 HLA-A2⁺ cell lines of different tissue origins, unless preloaded with mutant peptide, suggesting a high degree of peptide and HLA specificity (Fig. 1g).

Fig. 2 | TCR^{FLT3D/Y} cells efficiently kill primary AML cells harboring the FLT3^{D835Y} mutation in vitro but spare normal lymphoid cells. **a**, Percentage myeloid cells of live leukocytes for patients (Pt.) 1–8 with AML; gating strategy is shown in Extended Data Fig. 6a. Dots represent technical replicates from one representative experiment as described in **d**. **b**, PB or BM FLT3^{D/Y} VAF for patients 1–8 as determined by next-generation sequencing. **c**, Representative t-distributed stochastic neighbor embedding (t-SNE) plots showing live primary myeloid cells (CD3[−]CD19⁺CD20[−] events) in red, T cells (CD3⁺) in blue, B cells (CD19⁺CD20⁺) in orange and normal CD34⁺lin[−] progenitor cells in green from $n=3$ representative HLA-A2⁺ FLT3^{D/Y} patients (patients 2, 3 and 6) with AML and one HLA-A2[−] FLT3^{D/Y} patient (patient 8) following 72 h of co-culture with TCR^{1G4} (negative control, top) or TCR^{FLT3D/Y} cells (E:T ratio, 1:2) as quantified by flow cytometry. Cells transduced to express TCR were excluded from analysis as CellTrace Violet (CTV)-positive events. **d**, Diagnostic samples from 11 patients

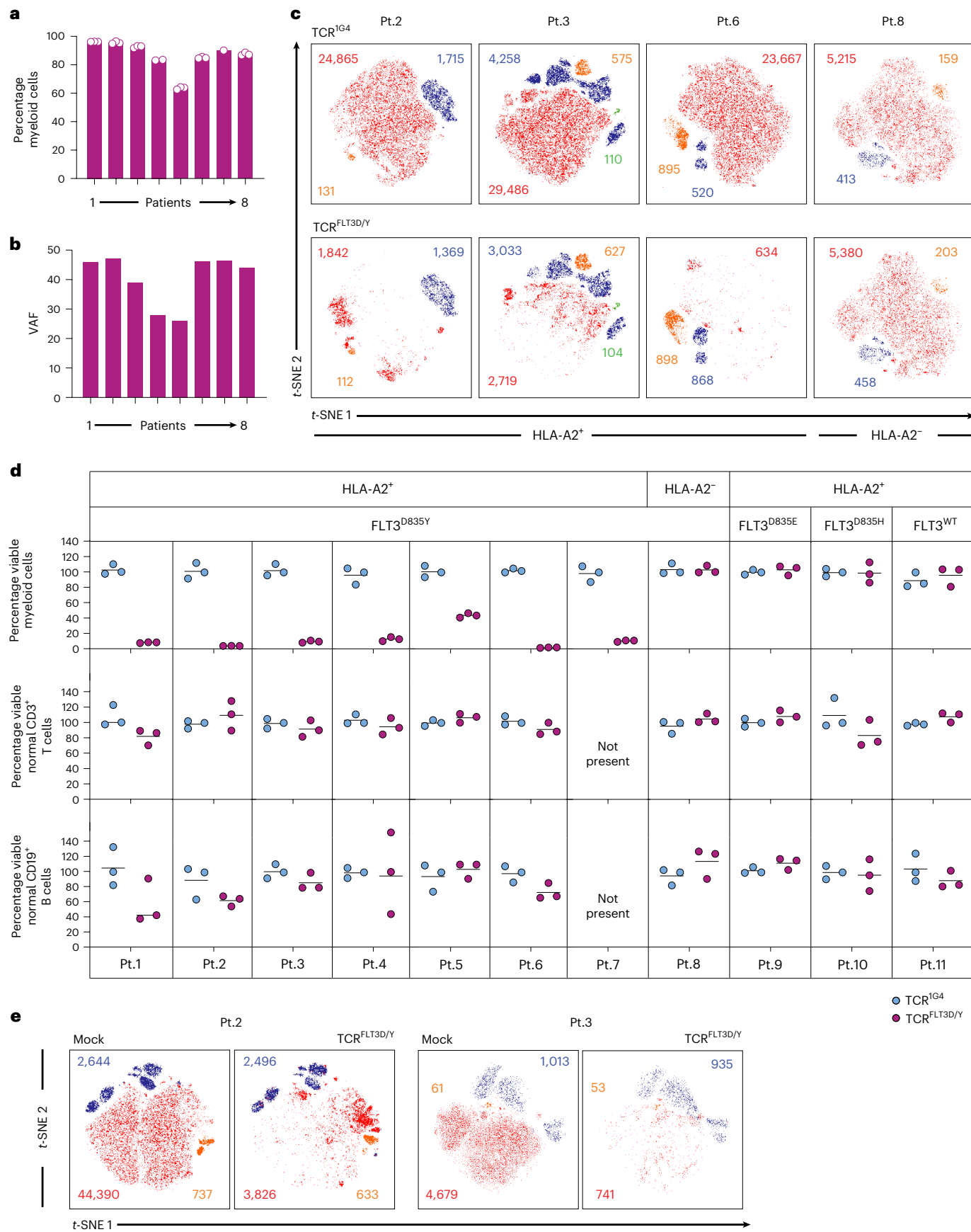
We next mapped the fine specificity of TCR^{FLT3D/Y}. TCR^{FLT3D/Y} cells were screened for interferon (IFN)-γ production in response to target cells loaded with each peptide in a library of 161 peptides representing single-amino acid-substituted variants of the cognate peptide (Fig. 1h and Extended Data Fig. 4a). Peptide motifs harboring any ‘permitted’ alternative amino acids in each position were queried in the human proteome databases UniProtKB/Swiss-Prot by employing the ScanProsite tool (<https://prosite.expasy.org/scanprosite/>) (Extended Data Fig. 4b), identifying 28 additional 9-mers in the human proteome potentially recognized by TCR^{FLT3D/Y} cells (Supplementary Table 1). However, only three of these peptides (peptide 11, AVISDAMYI, derived from LZTR1; peptide 12, YITSDMFYV, derived from MED1; and peptide 15, AVDNDSFYV, derived from PRADCI) activated TCR^{FLT3D/Y} cells (Fig. 1i). The three genes encoding proteins harboring the potentially cross-reactive peptide sequences are ubiquitously expressed according to the HPA database (<https://www.proteinatlas.org/>). A lack of reactivity observed in response to the panel of 26 HLA-A2⁺ cell lines (Fig. 1g) therefore suggested that the peptides are not processed and presented. To further exclude this, we generated mRNA constructs encoding 30-mer peptides with the cross-reactive peptide in the middle flanked by the natural respective protein sequences and a green fluorescent protein (GFP) reporter (Extended Data Fig. 4c). Co-cultures demonstrated that TCR^{FLT3D/Y} cells did not react to K562 HLA-A2⁺ target cells electroporated with the mRNA constructs encoding peptides derived from LZTR1, MED1 or PRADCI (Fig. 1j and Extended Data Fig. 4d), indicating that these peptides are not naturally processed and presented on HLA-A2. In agreement with this, none of the 28 candidate peptides were found in the HLA ligand database⁴³.

TCR^{FLT3D/Y} cells kill primary FLT3^{D835Y} AML cells in vitro

Reanalysis of publicly available DNA sequencing data of 49 patients with AML and the FLT3^{D835Y} mutation¹⁵ demonstrated that the FLT3^{D835Y}-mutated clone is frequently dominant (Extended Data Fig. 5a). The FLT3^{D835Y} mutation had the highest variant allele frequency (VAF) among identified recurrent driver single-nucleotide variants (SNVs) and indels in 22 patients (45%). In two additional patients, it was only preceded by a recurrent SRSF2 and TET2 mutation, known to occur in normal individuals with clonal hematopoiesis (CH) and requiring additional driver mutations to transform to AML⁴⁴. Similarly, reanalysis of single-cell DNA-sequenced AMLs showed in two of nine patients with the FLT3^{D835Y} mutation that it had the highest VAF or was secondary only to CH-associated mutations⁴⁵ (Extended Data Fig. 5b). In sum, this analysis of 58 FLT3^{D835Y}-mutated patients with AML indicates that FLT3^{D835} is frequently clonal and that it might constitute an AML-initiating or transforming mutation.

We next explored the specificity and efficacy with which TCR^{FLT3D/Y} cells killed AML cells from 11 patients (Supplementary Table 2). DNA sequencing of mononuclear samples dominated by myeloid cells (Fig. 2a and Extended Data Fig. 6a) showed high FLT3^{D835Y} clonal

with AML and the FLT3^{D/Y} (patients 1–8), FLT3^{D/E} (patient 9) or FLT3^{D/H} (patient 10) mutation or FLT3^{WT} (patient 11) (all HLA-A2⁺ except patient 8), analyzed as described in **c**. Each dot represents the fraction of live myeloid cells, B cells or T cells after co-culture with TCR^{FLT3D/Y} cells (purple) in percent mean of the corresponding numbers in cultures treated with TCR^{1G4} cells (blue). Data points represent $n=3$ technical replicates, and horizontal lines show means. Data shown are from one experiment representative of two to four experiments performed for each patient sample ($n=1$ only for patient 7). **e**, t-SNE plots of PB diagnostic samples from patients 2 and 3 with AML showing live myeloid, T and B cells (color coded as in Fig. 2c) after 72 h of co-culture with autologous T cells transduced to express TCR^{FLT3D/Y} or the mock control. Inset numbers in **c,e** denote absolute event counts of the indicated cell populations. The gating strategy is shown in Extended Data Fig. 6e.



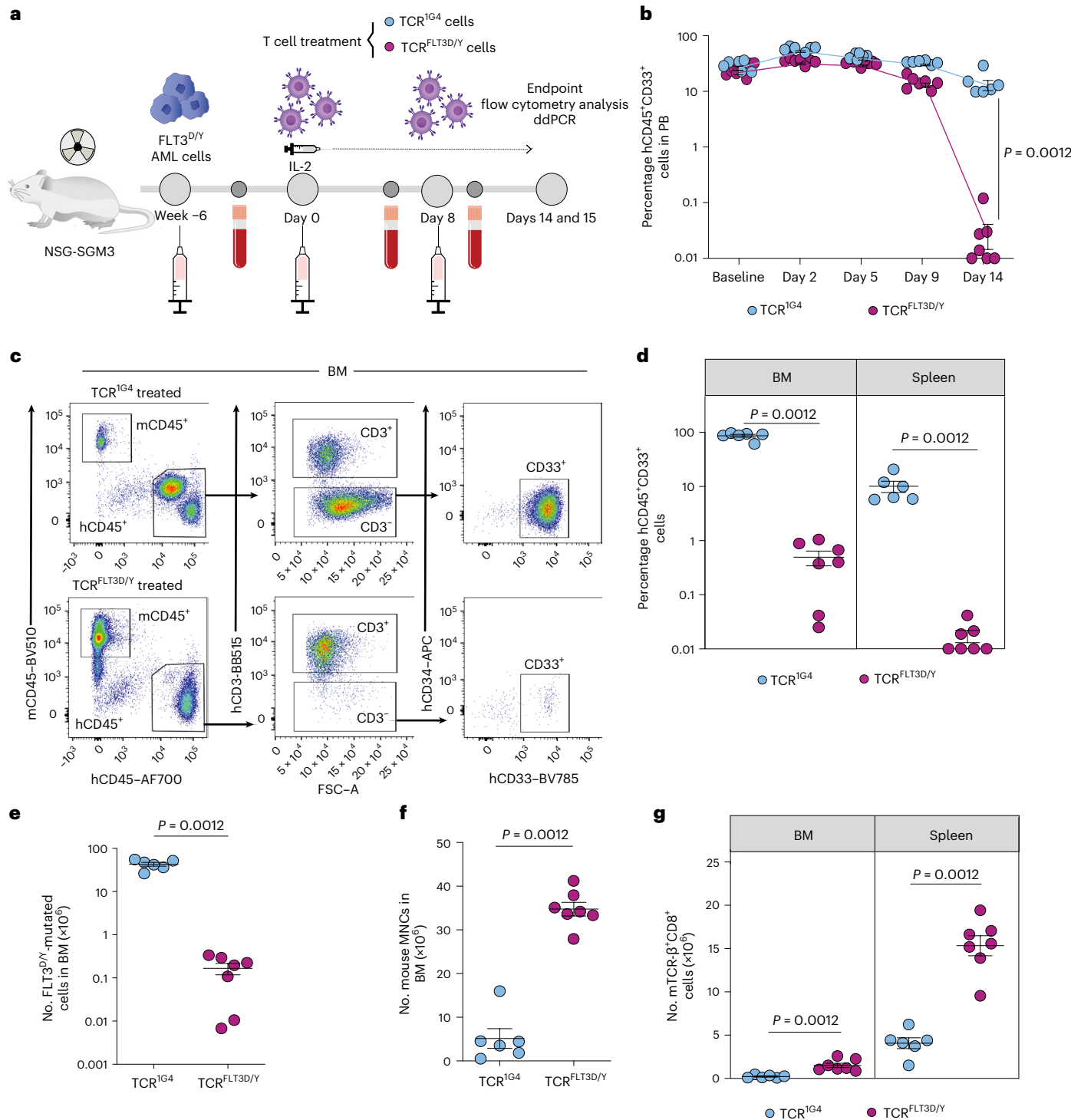


Fig. 3 | TCR^{FLT3D/Y} cells efficiently target primary AML in mice with high leukemic burden. **a**, Schematic overview of the PDX in vivo model with FLT3^{D835Y}-mutated primary AML cells from patient 7. **b**, Percentage of human hCD45⁺CD33⁺ cells in PB at baseline (1 d before T cell infusion) and on the indicated days after infusion with TCR^{1G4} ($n = 6$ mice) or TCR^{FLT3D/Y} ($n = 7$ mice) cells. Numbers were adjusted for hCD3⁺ T cells. **c**, Representative flow cytometry plots of viable single BM mononuclear cells (MNCs) from TCR^{1G4} (top) and TCR^{FLT3D/Y} (bottom) cell-treated NSG-SGM3 mice stably engrafted with primary AML FLT3^{D/Y} cells from patient 7. **d**, Percentage of hCD45⁺CD33⁺ cells in the

BM and spleen at terminal analysis 15 d after T cell infusion. Numbers were adjusted for hCD3⁺ T cells. **e**, Number of FLT3^{D835Y}-mutated BM hCD45⁺CD3⁻ cells determined by ddPCR. **f,g**, Number of mouse (m)CD45⁺ cells in BM (**f**) and mTCR-β'CD8⁺ cells in the BM and spleen (**g**) at the endpoint. All data are presented as mean \pm s.e.m. and were generated from one experiment including six mice treated with TCR^{1G4} cells and seven mice treated with TCR^{FLT3D/Y} cells. Each dot represents one mouse, and statistical analysis was performed with two-tailed Mann-Whitney test. P values are shown, and $P < 0.05$ was considered statistically significant.

involvement in the eight $\text{FLT3}^{\text{D835Y}}$ patients (Fig. 2b and Supplementary Table 3). $\text{TCR}^{\text{FLT3D/Y}}$ cells killed myeloid cells from patients 1–7 with AML effectively at effector:target (E:T) ratios as low as 1:2 (mean, 87%; range, 53.3–98.7%, Fig. 2c,d). CD3⁺ T cells and CD19⁺CD20⁺ B cells were not significantly affected (Fig. 2c,d and Extended Data Fig. 6b), as expected in view of low clonal involvement⁴⁶. However, B cell counts were very low (Extended Data Fig. 6a,b), and we therefore also investigated the effect of $\text{TCR}^{\text{FLT3D/Y}}$ cells on isolated B cells from healthy donors, which demonstrated a lack of killing (Extended Data Fig. 6c). The HLA restriction of $\text{TCR}^{\text{FLT3D/Y}}$ was confirmed by lack of killing of myeloid HLA-A2[−] $\text{FLT3}^{\text{D835Y}}$ patient cells (patient 8; Fig. 2c,d). Specificity for the D835Y substitution of FLT3 was demonstrated by lack of recognition of AML samples with alternative amino acid substitutions in the D835 position (patients 9 and 10) or expressing FLT3^{WT} (patient 11) (Fig. 2d and Supplementary Table 2). Robust and specific IFN- γ production was observed upon co-incubation of $\text{TCR}^{\text{FLT3D/Y}}$ cells with HLA-A2⁺ $\text{FLT3}^{\text{D835Y}}$ patient cells (patients 1–6; Extended Data Fig. 6d). Finally, $\text{TCR}^{\text{FLT3D/Y}}$ cells derived from patients with AML killed autologous leukemia cells with similar efficacy and selectivity as third-party T cells, mimicking the clinical setting (Fig. 2e and Extended Data Fig. 6e). In most cases, two to four experiments were performed per patient sample, with only one experiment performed due to a limited amount of material in a few instances, as described in the figure legends.

$\text{TCR}^{\text{FLT3D/Y}}$ cells efficiently target human leukemia cells in vivo

We initially investigated whether $\text{TCR}^{\text{FLT3D/Y}}$ cells recognized endogenously presented antigen in a small experiment using an *in vivo* xenograft mouse model engrafted with a leukemia cell line. Because $\text{FLT3}^{\text{D835Y}}$ leukemic cell lines are not commercially available, we introduced the mutation into different leukemia cell lines and demonstrated that $\text{TCR}^{\text{FLT3D/Y}}$ cells killed >95% of leukemic cells in 24 h at low E:T ratios (1:2) (Extended Data Fig. 7a,b). BV173 $\text{FLT3}^{\text{D835Y}}$ -expressing cells (cell line origin, B cell precursor leukemia) were next transplanted into NOD.Cg-*Prkdc*^{scid} *Il2rg*^{tm1Wjl}/SzJ (NSG) mice (Extended Data Fig. 7c,d). All mice in the control groups (untreated ($n = 3$) and TCR^{IG4} cells ($n = 3$)) were killed after 21 d due to high leukemic burden, at which time leukemic cells were undetectable in the $\text{TCR}^{\text{FLT3D/Y}}$ cell-treated group ($n = 4$) (Extended Data Fig. 7e,f). Among four mice receiving the therapeutic TCR, two survived for the duration of the experiment (53 d) and one remained free of leukemia but was killed on day 41 due to graft-versus-host disease, whereas one relapsed on day 28 and was found dead on day 32 (Extended Data Fig. 7e). Upon termination, no leukemic cells were detected in the bone marrow (BM) of the two surviving $\text{TCR}^{\text{FLT3D/Y}}$ cell-treated mice (Extended Data Fig. 7g,h), while transduced T cells in the BM persisted (Extended Data Fig. 7i).

$\text{TCR}^{\text{FLT3D/Y}}$ cells efficiently eliminate primary AML in PDX models

To investigate the *in vivo* efficacy of $\text{TCR}^{\text{FLT3D/Y}}$ cells in disease-relevant models, we next treated mice engrafted with primary AML cells in different PDX models.

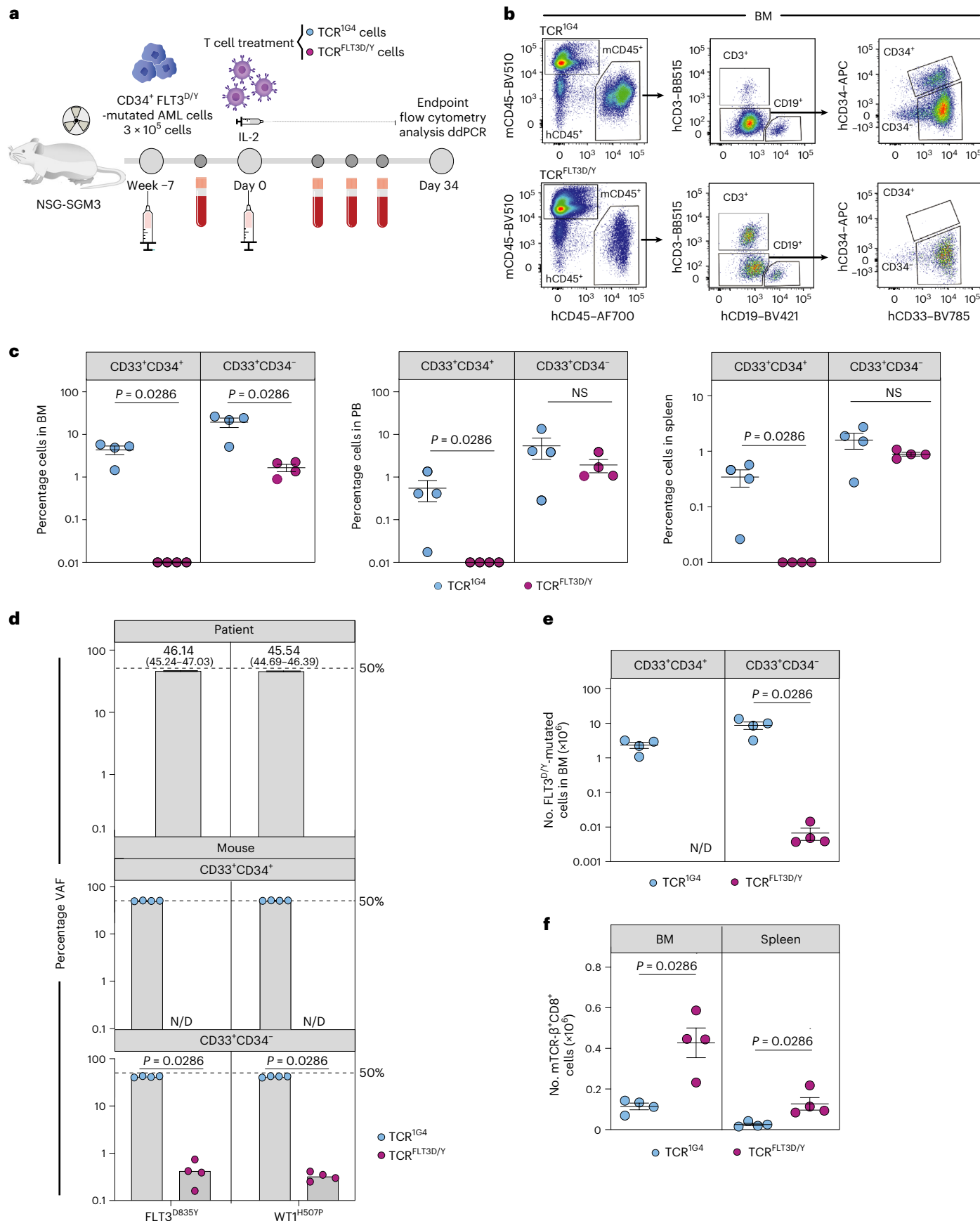
Fig. 4 | $\text{TCR}^{\text{FLT3D/Y}}$ cells eliminate primary CD34⁺ AML in vivo. a, Schematic overview of the PDX *in vivo* model with $\text{FLT3}^{\text{D835Y}}$ -mutated primary AML cells from patient 1. **b**, Representative flow cytometry plots of BM from TCR^{IG4} (top) and $\text{TCR}^{\text{FLT3D/Y}}$ (bottom) cell-treated NSG-SGM3 mice stably engrafted with primary AML $\text{FLT3}^{\text{D/Y}}$ cells from patient 1. Equivalent gating was also used for PB and the spleen. **c**, Percentage of hCD45⁺CD33⁺CD34⁺ and hCD45⁺CD33⁺CD34[−] cells in the BM, PB and spleen at the endpoint (day 34 after T cell infusion) of TCR^{IG4} ($n = 4$ mice) or $\text{TCR}^{\text{FLT3D/Y}}$ ($n = 4$ mice) cell-treated mice. Numbers were adjusted for hCD3⁺ T cells. NS, not significant. **d**, Percentage VAF determined by ddPCR of $\text{FLT3}^{\text{D835Y}}$ and $\text{WT1}^{\text{H507P}}$ driver mutations in primary BM cells from patient 1 (top) and hCD45⁺CD33⁺CD34⁺ (middle) and hCD45⁺CD33⁺CD34[−] (bottom) cells from TCR cell-treated mice. N/D, not analyzed due to insufficient hCD45⁺CD33⁺CD34⁺

Model 1. NSG-SGM3 mice highly engrafted with primary $\text{FLT3}^{\text{D835Y}}$ AML cells from patient 7 (24.5% ± 2.2% human CD33⁺ cells in PB) (Fig. 3a,b and Supplementary Tables 2 and 3) were treated with $\text{TCR}^{\text{FLT3D/Y}}$ ($n = 7$) or control TCR^{IG4} ($n = 6$) cells. Serial analysis of PB demonstrated a maintained high CD33⁺ engraftment in TCR^{IG4} -treated mice, whereas CD33⁺ cells were virtually eliminated by day 14 in all $\text{TCR}^{\text{FLT3D/Y}}$ -treated mice (Fig. 3b and Extended Data Fig. 8a). Mice were closely monitored for potential allo-reactivity mediated by endogenous TCRs of the T cells transduced to express TCR derived from a third-party donor, which could otherwise confound the anti-tumor reactivity mediated by $\text{TCR}^{\text{FLT3D/Y}}$. Thus, terminal analysis of all TCR^{IG4} -treated and $\text{TCR}^{\text{FLT3D/Y}}$ -treated mice was performed on day 15 after T cell infusion when tumor burden started to decline slightly also in control mice (Fig. 3b). BM analysis demonstrated high CD33⁺ AML engraftment in TCR^{IG4} -treated mice (mean, 86.9% ± 5.3%), which was reduced to a mean of 0.5% ± 0.2% in $\text{TCR}^{\text{FLT3D/Y}}$ -treated mice, with a similar reduction in the spleen (Fig. 3c,d and Supplementary Table 4). An almost complete elimination of $\text{FLT3}^{\text{D/Y}}$ AML cells in the BM was confirmed by droplet digital PCR (ddPCR) analysis, quantifying clonally involved cells (Fig. 3e and Supplementary Table 5). Importantly, efficient targeting of human AML cells in $\text{TCR}^{\text{FLT3D/Y}}$ -treated mice resulted in recovery of mouse hematopoiesis, which was severely suppressed by high leukemic burden in TCR^{IG4} -treated mice (Fig. 3f and Extended Data Fig. 8b,c). T cells transduced to express TCR were detected in the BM, spleen and PB of all mice throughout the experiment (Fig. 3g and Extended Data Fig. 8d–g).

Model 2. Primary xenografts from a second $\text{FLT3}^{\text{D835Y}}$ -mutated AML sample engrafted in NSG-SGM3 mice (patient 1, Supplementary Table 2) were investigated for response to $\text{TCR}^{\text{FLT3D/Y}}$ cells (Fig. 4a). Unlike patient 7 (Fig. 3c), this AML co-expressed CD34, a stem and progenitor marker characteristic of CD34⁺ AMLs⁴⁷, for which CD34⁺ cells in contrast to CD34[−] cells have been shown to possess leukemia-propagating activity^{48,49}. Control TCR-treated mice had relatively low levels of PB human CD33⁺ engraftment 34 d after T cell injection (mean, 6.0% ± 3.1% human (h)CD45⁺CD33⁺ cells), whereas BM engraftment was much higher (mean, 23.7% ± 5.8%) (Fig. 4b, Extended Data Fig. 9a,b and Supplementary Table 6). In $\text{TCR}^{\text{FLT3D/Y}}$ -treated mice, this was reduced to 1.9% ± 0.7% in PB and 1.7% ± 0.3% in the BM (Extended Data Fig. 9a,b). Terminal BM analysis on day 34 after T cell injection revealed distinct populations of CD33⁺CD34[−] (mean, 19.4% ± 4.8%) and CD33⁺CD34⁺ cells (mean, 4.4% ± 1.0%) in control TCR^{IG4} -treated mice (Fig. 4b,c). In $\text{TCR}^{\text{FLT3D/Y}}$ -treated mice, some CD33⁺CD34[−] cells persisted in the BM although at greatly reduced levels (mean 1.7% ± 0.3%), whereas CD33⁺CD34⁺ cells were completely eliminated. Similar findings were observed in PB and the spleen (Fig. 4c and Supplementary Table 6).

DNA sequencing confirmed that cells engrafted in NSG-SGM3 mice were represented by the same exonic mutations as those detected in AML blasts from the BM of patient 1, with $\text{FLT3}^{\text{D835Y}}$ and $\text{WT1}^{\text{H507P}}$ representing the only detected recurrent driver mutations (Supplementary Table 7). Further quantification by ddPCR demonstrated

cells. Numbers show VAF and 95% confidence intervals. The dashed line at 50% indicates 100% clonality unless loss of heterozygosity. No significant differences in VAFs of the $\text{FLT3}^{\text{D835Y}}$ and $\text{WT1}^{\text{H507P}}$ mutations were observed. **e**, Number of $\text{FLT3}^{\text{D835Y}}$ -mutated hCD45⁺CD33⁺CD34⁺ and hCD45⁺CD33⁺CD34[−] cells in the BM as determined by ddPCR. N/D, not detected due to lack of hCD45⁺CD33⁺CD34⁺ cells. **f**, Number of mTCR- β ⁺CD8⁺ cells in the BM and spleen at the endpoint. All data are presented as mean ± s.e.m. from terminal analysis 34 d after T cell infusion from one experiment including four mice treated with TCR^{IG4} cells and another four mice treated with $\text{TCR}^{\text{FLT3D/Y}}$ cells. Each dot represents one mouse, and statistical analysis was performed with two-tailed Mann–Whitney test. *P* values are shown, and *P*<0.05 was considered statistically significant.



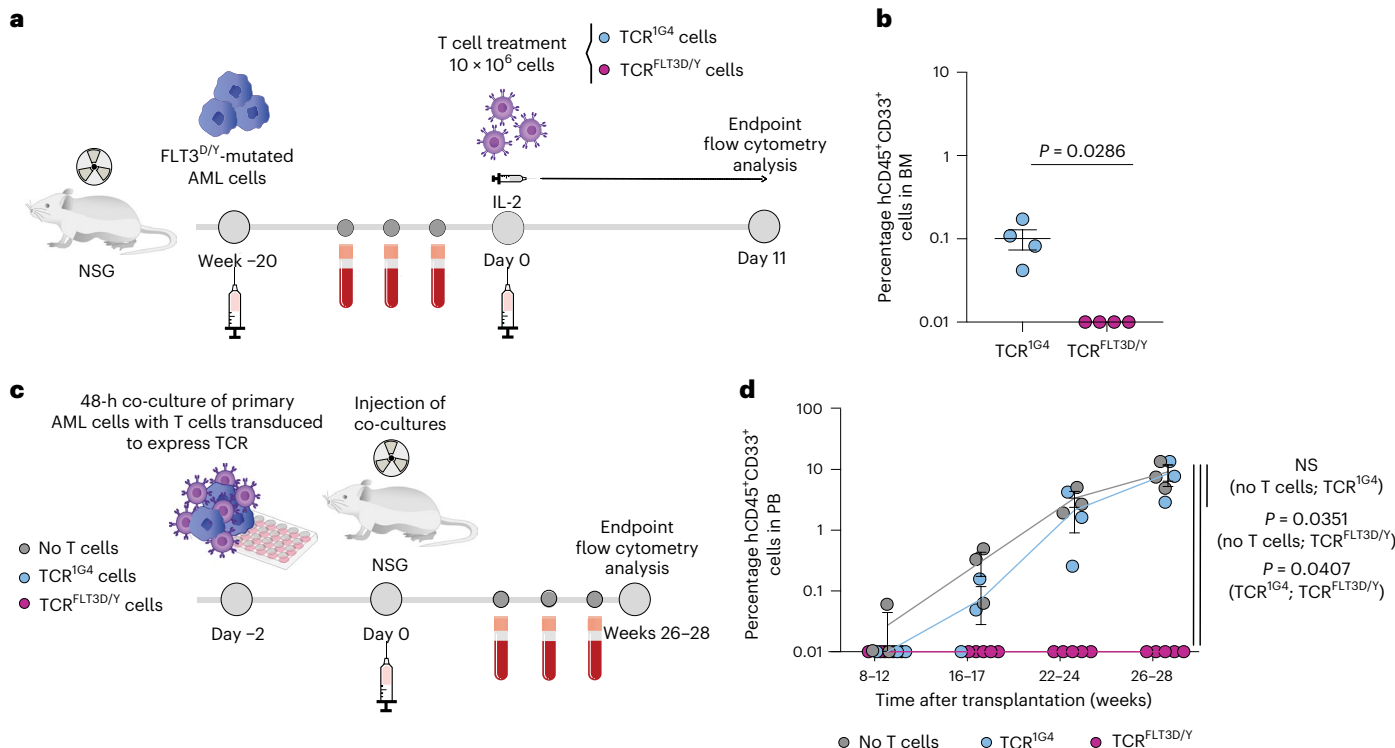


Fig. 5 | TCR^{FLT3D/Y} cells efficiently kill primary AML in an MRD setting and eliminate leukemia-propagating cells. **a**, Schematic overview of the MRD PDX in vivo model with FLT3^{D835Y}-mutated primary AML cells from patient 1. **b**, Percentage of hCD45⁺CD33⁺ cells in the BM of NSG mice engrafted with low levels of AML after treatment with TCR^{1G4} ($n = 4$ mice) or TCR^{FLT3D/Y} ($n = 4$ mice) cells 11 d after T cell infusion. Numbers were adjusted for hCD3⁺ T cells. Data are presented as mean \pm s.e.m. and were generated from one experiment. Each dot represents one mouse, and statistical analysis was performed with two-tailed Mann–Whitney test. **c**, Schematic overview of the PDX in vivo model

with FLT3^{D835Y}-mutated primary AML cells from patient 1 after in vitro targeting with TCR^{1G4} or TCR^{FLT3D/Y} cells. **d**, Percentage of hCD45⁺CD33⁺ cells in PB at the indicated time after transplantation of primary AML cells from patient 1 following 48 h of co-culture without T cells ($n = 3$ mice) or with TCR^{1G4} ($n = 3$ mice) or TCR^{FLT3D/Y} ($n = 5$ mice) cells. Data are presented as mean \pm s.e.m. and were generated from two independent experiments. Each dot represents one mouse, and statistical analysis was performed by multilevel linear regression using the R package ‘lmerTest’ (further described in the Methods). P values are shown, and $P < 0.05$ was considered statistically significant.

that FLT3^{D835Y} and WT1^{H507P} mutations represented the dominating clone, with a VAF > 45% in patient 1 as well as in engrafted NSG-SGM3 mice (Fig. 4d). Notably, among the remaining CD33⁺CD34⁺ BM cells of TCR^{FLT3D/Y}-treated mice, the fraction of FLT3^{D835Y}-mutated cells was reduced to only 0.9% \pm 0.3% as compared with 83.4% \pm 2.1% in TCR^{1G4}-treated mice. This translates into more than a 1,300-fold reduction in CD33⁺CD34⁺ FLT3^{D/Y} AML cells in TCR^{FLT3D/Y}-treated mice (Fig. 4d,e, Extended Data Fig. 9c and Supplementary Table 8). Human T cells including T cells transduced to express TCR were detected in the BM, spleen and PB of all treated mice throughout the course of the experiment (Fig. 4f and Extended Data Fig. 9d–g). Cells from patient 1 also reconstituted CD19⁺ B lymphocytes in engrafted mice (Fig. 4b), and, in agreement with previous studies⁴⁶, these were not part of the FLT3^{D/Y} leukemic clone (Extended Data Fig. 9c and Supplementary Table 8).

Model 3. To establish a PDX model mimicking minimal residual disease (MRD)⁵⁰, secondary transplantations of mice engrafted with AML cells from patient 1 were performed into NSG mice, a mouse strain that, in contrast to NSG-SGM3 mice, does not specifically enhance human myeloid lineages. In accordance with results from the NSG-SGM3 model, we observed efficient elimination of FLT3^{D/Y} primary AML cells also in this MRD setting (Fig. 5a,b and Supplementary Table 9).

Model 4. TCR^{FLT3D/Y} treatment resulted in undetectable levels of CD34⁺FLT3^{D/Y} AML cells in the PB, spleen and BM of all mice engrafted with AML cells from patient 1, compatible with complete elimination of

FLT3^{D/Y} AML-propagating cells in vivo through specific TCR^{FLT3D/Y} targeting. More definitive support for this would, however, require longer follow-up of mice to allow for potential outgrowth of rare and therapy-resistant AML stem cells that might have escaped T cell recognition. A long follow-up time was not possible in models 1–3 due to the continued presence of TCRT T cells having endogenous TCR repertoires that cause allo-reactivity and xenoreactivity over time. Moreover, to establish whether all AML-propagating cells have been eliminated by TCR^{FLT3D/Y} cells requires assessment in the absence of TCR^{FLT3D/Y} T cells. To circumvent these limitations, AML cells from patient 1 were cultured with TCR^{FLT3D/Y} or TCR^{1G4} cells or without T cells in vitro for 48 h before transplantation into NSG mice (Fig. 5c). The very few human T cells to which the AML cells were exposed in vitro did not persist in vivo (Extended Data Fig. 10). The mice did not receive interleukin (IL)-2 infusions. Potential AML development could therefore be followed for 28 weeks. During this time, mice injected with AML cells from control cultures without T cells or with control TCR^{1G4} cells showed progressive and high leukemic engraftment. By contrast, no detectable engraftment was observed at any time in any mice transplanted with AML cells co-cultured with TCR^{FLT3D/Y} cells (Fig. 5d and Extended Data Fig. 10). Collectively, these experiments demonstrate that TCR^{FLT3D/Y} cells can efficiently target and eliminate FLT3^{D835Y}-mutated in vivo AML-propagating cells.

Discussion

In this study, we identify a TCR recognizing an epitope from the recurrent driver mutation D835Y in the tyrosine kinase domain of FLT3 in

AML, presented on the prevalent HLA-A2 allele. This TCR, selected from healthy donor T cell repertoires, mediated highly specific and efficient killing of primary AML cells harboring the $\text{FLT3}^{\text{D835Y}}$ mutation in vitro and in vivo. Different clinically relevant aspects of therapeutic effects were demonstrated in different in vivo mouse PDX models. This included an almost complete removal of mutated CD34^- AML in model 1 with high engraftment and complete removal of CD34^+ AML in model 2 with lower levels of reconstitution. In a third PDX model, $\text{TCR}^{\text{FLT3D/Y}}$ cells rejected patient AML cells in a setting resembling MRD. $\text{TCR}^{\text{FLT3D/Y}}$ cells thus efficiently eliminated leukemia with both high and low disease burden. AML cells that are CD34^+ have previously been shown to propagate leukemia in vivo⁴⁹. Here, we demonstrated, in a fourth PDX model followed for 7 months after AML injection, that $\text{TCR}^{\text{FLT3D/Y}}$ cells in vitro can specifically and efficiently target and kill leukemia-propagating CD34^+ $\text{FLT3}^{\text{D835Y}}$ -mutated AML cells. Studies in humans would, however, be required to confirm that $\text{TCR}^{\text{FLT3D/Y}}$ cells could achieve this also in vivo. In sum, this suggests that a therapeutic TCR targeting a single, shared neoantigen has the potential of eliminating the reservoir of leukemia stem cells in AML.

The prospect of treating large patient groups with cytotoxic T cells expressing a single TCR targeting public neoantigens expressed by prevalent HLA molecules has emerged as an attractive therapeutic possibility⁵¹. However, although a large number of recurrent hotspot mutations are known, it has proven difficult to identify HLA-bound peptides from tumor samples by immunopeptidomics^{52,53}. One reason might be that driver mutations that are poorly presented to the immune system provide a survival advantage. Another possibility is that mass spectrometry has insufficient sensitivity for detection of many neoantigenic peptides. We were, however, able to identify the $\text{FLT3}^{\text{D/Y}}$ neoepitope in two AML patient samples by targeted mass spectrometry, starting with a large number of leukemia cells. T cells are, on the other hand, the most sensitive tools available for detection of pMHC complexes⁵⁴. Our technology using mRNA-transduced dendritic cells to prime naive T cells from healthy donors provides the means to identify neoepitopes and reactive TCRs in a single assay^{38,39}. Presentation of the $\text{FLT3}^{\text{D/Y}}$ neoepitope on leukemic cells was confirmed by efficient killing of primary HLA-A2⁺ AML cells expressing $\text{FLT3}^{\text{D835Y}}$, but not the less frequent $\text{FLT3}^{\text{D835E}}$ or $\text{FLT3}^{\text{D835H}}$ mutations or FLT3^{WT} , by $\text{TCR}^{\text{FLT3D/Y}}$ cells, further demonstrating TCR specificity.

To date, most efforts to isolate neoantigen-specific TCRs employ strategies in which memory T cell responses in patient material are interrogated^{11,55,56}. Identification of TCRs with sufficient affinity is essential for clinical impact^{41,57}. A hurdle might be induction of T cell tolerance due to long-standing co-evolution between cancer and the immune system in the absence of inflammation and lack of sufficient priming. This might contribute to the low spontaneous reactivity that tumor-infiltrating T cells show to the large repertoire of predicted neoantigens in melanoma¹¹. In support of this, immune responses to neoantigen vaccines seem to be dominated by de novo responses induced in naive T cells^{58–60}. The possibility of inducing neoantigen-specific responses from naive patient-derived T cells is, however, limited by the amount of blood that can be collected and by T cell repertoires that might be reduced by foregoing therapy. In an earlier study, we showed that healthy donor-derived T cells recognized fivefold more neoantigens than tumor-infiltrating lymphocytes of patients with melanoma³⁸. Here, we used the same approach to identify $\text{TCR}^{\text{FLT3D/Y}}$, which recognizes peptide at picomolar concentrations and mediates efficient cytotoxicity against primary AML cells in vitro and in vivo. High antigen sensitivity, indicated by EC_{50} values below 10 nM, appears to be an important factor for TCRs in effectively killing cancer cells, as previously demonstrated by us²⁷ and others^{9,41,61,62}. Similarly, Foy et al., in their publication in *Nature*, discussed the potential association between low EC_{50} values observed for personalized neoantigen-reactive TCRs in their study and the limited clinical efficacy observed¹².

We primed T cells from 16 healthy donors to identify T cells recognizing the YIMSDSNYV peptide presented by HLA-A2. This indicates low immunogenicity of the peptide, consistent with lack of recognition by the investigated AML patient T cells, although a limited number of cells were screened for reactivity. In sum, this demonstrates the advantage of accessing large, healthy donor T cell repertoires. We previously demonstrated that peptide-HLA stability is an important predictor of neoantigen immunogenicity³⁸. Here, we showed that the off-rate for the $\text{FLT3}^{\text{D835–843}}$ peptide bound to HLA-A2 was significantly slower when substituting the WT amino acid D in position 1 with a Y. This is consistent with other studies showing that increased stability of the neoantigen relative to the corresponding WT peptide leads to sustained antigen presentation and increased T cell recognition^{63,64}. Testing for potential off-target reactivity is essential to detect possible safety concerns before clinical use⁶⁵. Mapping of TCR fine specificity using a library of single-amino acid-substituted peptides followed by a bioinformatic screen did not identify cross-recognized peptides, although this does not completely exclude potential recognition of peptide sequences that are unrelated to the cognate peptide. $\text{TCR}^{\text{FLT3D/Y}}$ cells did not, however, react to a panel of 26 HLA-A2⁺ cell lines of different tissue origins and spared normal blood cells and AML cells expressing the FLT3^{WT} sequence or alternative $\text{FLT3}^{\text{D835}}$ mutations.

Treatment with $\text{TCR}^{\text{FLT3D/Y}}$ cells would be limited to the 3–4% of patients that, in addition to expressing the mutation also express HLA-A2 in the European-descended population³². While recurrent FLT3 mutations are frequently known to represent secondary and accelerating AML mutations^{15,33,66}, our reanalysis of 58 published $\text{FLT3}^{\text{D835Y}}$ -mutated AML patient samples^{15,45} demonstrated that this FLT3 mutation frequently is clonal and, in some cases, also might be the initiating mutation or secondary only to a CH mutation. These data are in agreement with the high VAF for $\text{FLT3}^{\text{D835Y}}$ in all included patients with AML harboring this mutation, where the only selection criterion upfront was the presence of the mutation. In sum, this highlights the therapeutic and potentially curative potential of eradicating $\text{FLT3}^{\text{D835Y}}$ -mutated AML clones. Furthermore, in cases in which TKIs effectively target FLT3 ITD but select for AML subclones with FLT3 point mutations, including $\text{FLT3}^{\text{D835Y}}$, resistant to first-generation as well as second-generation TKIs^{35–37}, $\text{FLT3}^{\text{D835Y}}$ -mutation-specific TCR treatment could be combined with TKIs. As part of a paradigm in which combination regimens are tailored based on tumor molecular profiles, TCR therapies targeting specific recurrent point mutations provide a potential means for highly efficacious eradication of specific tumor clones.

TCRs can access recurrent mutations currently inaccessible to CARs. Moreover, TCRs might have inherent advantages relative to CARs that improve T cell persistence and antigen sensitivity⁶⁷. Today, TCR-based therapies are mostly applied in the form of genetically modified T cells, although soluble bispecific TCR engagers have emerged as new opportunities for off-the-shelf therapies at lower cost⁶⁸. The results presented here show that a TCR targeting a single shared neoantigen generated from a healthy donor can provide highly efficacious and specific cancer treatment in vivo in multiple disease-relevant models, paving the way for future off-the-shelf, tumor-specific immunotherapies.

Methods

This study was approved by the Regional Committee for Medical and Health Research Ethics South-East Norway (2018/879, 2018/1246 and 2015/2357), the Institutional Review Board and the Data Protection Officer, Oslo University Hospital, the Swedish Ethical Review Authority, Stockholm (EPN 2017/2085-31/2) and the Ethical Committee in Central Denmark Region (1-45-70-88-21) and was performed in accordance with the Declaration of Helsinki. The Norwegian Food Safety Authority (application ID 17500) and Stockholms Djurförsöksetiska nämnd (17978-2018) approved all animal experiments.

Primary patient cells, healthy blood donor cells and cell lines

Buffy coats (PBMCs) from healthy donors were provided by the blood bank of Oslo University Hospital, and PB or BM MNCs from patients with leukemia were isolated from cryopreserved, biobanked material (ethical approvals 2018/879 and 2018/1246). MNCs derived by density-gradient centrifugation (Axis-Shield) were stained to determine HLA-A2 expression by flow cytometry. To confirm the presence of FLT3^{D835Y}, genomic DNA was extracted (QIAGEN DNeasy purification kit) from patient primary cells, and samples were sequenced using the TruSight Myeloid panel (Illumina). Information regarding the patients' sex (reported in Supplementary Table 2) was not considered during the design of the study but was part of the overall clinical information obtained at the hospital. No sex- or gender-based analysis was performed because each patient is shown individually in the study.

Epstein–Barr virus-transformed lymphoblastoid cell lines (EBV-LCL) were generated from HLA-A2⁺ and HLA-A2⁻ PBMCs as described previously²⁷. All other cell lines were gifted or obtained from the American Type Culture Collection (ATCC) or the German Collection of Microorganisms and Cell Cultures (DSMZ) as indicated in the Nature Portfolio Reporting Summary. Authentication was performed by short tandem repeat DNA profiling by Labcorp DNA Identification Lab (formerly Genetica, <https://celllineauthentication.com/>). Cell line cultures were grown in humidified cell incubators containing 5% CO₂ at 37 °C using media according to provider guidelines and were tested frequently for potential mycoplasma contamination.

Minigene design

For generation of T cell responses, a minigene was designed to encode predicted epitopes (<https://services.healthtech.dtu.dk/service.php?NetMHC-4.0>) containing the FLT3^{D835Y} mutation, codon optimized and synthesized by GenScript. Subsequently, it was cloned into the pClpA102 vector for in vitro mRNA transcription using the RiboMAX Large Scale RNA production system (Promega), as previously described^{69,70}. The minigene encoded the FLT3 amino acid sequence KICDFGLARYIMSDSNYVVRGNVRLARLP (FLT3^{D835Y} 9-mer and 10-mer are underlined and the mutation in position 1 is shown in bold).

Induction of antigen-specific T cells

Monocytes from HLA-A2⁺ healthy donors were isolated on day −4 using CD14-reactive microbeads and the autoMACS Pro Separator (Miltenyi Biotec). The CD14[−] PBMC fraction was cryopreserved for later use. The monocytes were then cultured for 3 d in CellGro GMP DC medium (CellGenix) with 1% (vol/vol) human serum (HS; Trina biotech), 1% (vol/vol) penicillin–streptomycin (P/S; Sigma-Aldrich), 50 IU ml^{−1} IL-4 (PeproTech) and 800 IU ml^{−1} GM-CSF (Genzyme). Subsequently, moDCs were matured for 14–16 h by adding lipopolysaccharide (Sigma-Aldrich) and IFN-γ (PeproTech) to final concentrations of 10 ng ml^{−1} and 100 IU ml^{−1}, respectively. On day −1, naïve CD8⁺ T cells were isolated from the autologous CD14[−] cryopreserved PBMCs by use of the autoMACS Pro Separator and a CD8⁺ T cell-isolation kit, into which CD45RO- and CD57-reactive beads (Miltenyi Biotec) were added. On day 0, moDCs were collected, electroporated with mRNA and co-cultured with naïve T cells in DC-T cell medium with 30 ng ml^{−1} IL-21 (PeproTech) at a DC:T cell ratio of 1:4. After 10 d, co-cultures were screened for the presence of FLT3^{D/Y} pMHC multimer-reactive CD8⁺ T cells. pMHC multimers labeled with PE and APC were prepared in house as described previously^{71,72}. Viable CD8⁺pMHC⁺ T cells (double positive for PE- and APC-conjugated pMHC multimers) were sorted by flow cytometry.

Expansion of memory T cells reactive to FLT3^{D/Y} in samples from patients with AML following HSCT

For in vitro expansion of potential memory T cells reactive to the FLT3^{D/Y}-mutant peptide in patients with AML that had undergone HSCT,

cryopreserved PB samples were thawed and resuspended in Iscove's Modified Dulbecco's Medium (IMDM) with 20% (vol/vol) FCS (Trina biotech) and 0.1 mg ml^{−1} DNase. Viable cells were resuspended at a concentration of 1 M ml^{−1} and pulsed with the FLT3^{D/Y} peptide at 100 ng ml^{−1} for 2 h at 37 °C. Cells were washed and resuspended at 3.75 million cells per ml in IMDM with 5% HS, 1× P/S and 20 U ml^{−1} IL-2 before culturing for 5 d. Identification of T cells reactive to the peptide was performed by staining with pMHC multimers as described above.

Sorting and cloning of pMHC multimer⁺CD8⁺ T cells

PBMCs from three healthy donors were mixed at an equal ratio (1:1:1) and irradiated with 35 Gy, washed and resuspended in X-VIVO 20 medium (Lonza, BioNordika) with 5% HS and 1% P/S (T cell medium). A total of 0.2 × 10⁶ irradiated cells (feeders) were placed into tissue culture-treated 96-well plates and were supplemented with 100 µl T cell medium containing 2 µg ml^{−1} phytohemagglutinin (Remel Thermo Scientific), 80 ng ml^{−1} IL-2 (R&D Systems) and 4 ng ml^{−1} IL-15 (PeproTech). FLT3^{D/Y} co-cultures were then collected and stained with LIVE/DEAD Fixable Near-IR, anti-CD3 antibody, anti-CD8a antibody and PE- and APC-conjugated pMHC multimers, and, using the FACSaria II (BD Biosciences) cell sorter, CD8⁺, pMHC-double-positive multimer populations were sorted as single cells into 96-well plates containing feeders. After 7 d, cultures were supplied with fresh T cell medium containing 1,750 U ml^{−1} IL-2 and 4 ng ml^{−1} IL-15, and expanding clones were identified by microscopy. On day 14, growing clones were restimulated with feeder cells prepared as described above and stained with FLT3^{D/Y} pMHC multimers. To assess functionality after expansion, clones were stimulated with K562 cells pulsed with FLT3^{D/Y} or FLT3^{WT} peptides and assessed for CD137 upregulation.

TCR sequencing

The sequences for paired TCR-α and TCR-β chains from two clones and 55 single cells reactive to FLT3^{D/Y} pMHC multimers were amplified as previously described but modified and adapted for the targeted amplification of transcripts encoding TCR-α and TCR-β (refs. 27,38,55). The MiXCR script was used to analyze sequencing data, and an in-house Python script TCR primer was used to reconstruct full-length TCR chains as described previously^{55,73}. The output was manually verified using IMGT/V-QUEST⁷⁴. For identified TCRs, codon-optimized sequences for TCR-α and TCR-β variable fragments were synthesized and cloned by GenScript.

Gene transfer to human PBMCs and cell lines

HLA-A2⁺ healthy donor-derived and patient-derived PBMCs were transduced to express FLT3^{D/Y}- and NY-ESO-1 (IG4)-specific TCRs, as detailed in ref. 27. Briefly, 2 × 10⁶ PBMCs per ml in CellGro GMP DC medium with 5% (vol/vol) HS, IL-7 and IL-15 (5 ng ml^{−1} each, PeproTech) were added to antibody-coated plates (anti-CD3 clone OKT3, eBioscience and anti-CD28 clone CD28.6, eBioscience) and incubated at 37 °C with 5% CO₂ for 72 h. Retroviral supernatants were generated as described previously²⁷. PBMCs were collected, resuspended in CellGro GMP DC medium with 5% HS, IL-7 and IL-15, mixed with retroviral supernatant, placed in non-tissue culture-treated six-well plates precoated with RetroNectin (20 µg ml^{−1}, Takara) and spinoculated at 900g for 60 min twice on consecutive days. Transduction efficiency was determined after 3 d by staining with anti-mouse TCR-β chain antibody and/or the pMHC multimer followed by flow cytometry. Before functional experiments, cells were cultured for 48–72 h in CellGro GMP DC medium containing low concentrations of cytokines (0.5 ng ml^{−1} IL-7 and IL-15). Alternatively, cells were frozen for later experiments.

BV173, ML-2, RS4;11 and NALM-6 cell lines were transduced as described above using retroviral supernatant containing the FLT3^{D/Y} minigene. For in vivo experiments, the BV173 cell line was stably transduced to express the FLT3^{D/Y} minigene, firefly luciferase and GFP

(hereafter, BV173^{D83SY}). Complementary DNA encoding FLT3^{D/Y} and HLA-A2 was cloned into the pCIP A102 vector for production of mRNA, as previously described^{70,71}

Immunoprecipitation-targeted mass spectrometry analysis of FLT3 peptides presented on HLA

Monoallelic B721.221 cells expressing HLA-A2 were transduced to express the mutant FLT3 amino acid sequence VLVTHGKVVKICDF GLARYIMSDSNYVVRGNARLPVK. One hundred million cells from the B721.221 line and 400 million cells from patient samples (patients 1 and 3) were lysed in PBS containing 1% lauryl maltoside, 0.5 mM EDTA, 1 mM PMSF and Sigma protease inhibitors (1:200) for 1 h at 4 °C (1 ml lysis buffer per 100 million cells). The clarified cell lysates were then added to 200 µl of AminoLink Plus bead slurry (Thermo Fisher Scientific) coated with pan-HLA class I-specific antibody (W6/32; BioXCell) to enrich for HLA peptides²⁷. The HLA-bound peptides were then sequentially eluted three times, each with 1 ml of 1% TFA. Peptide elutions were pooled and desalted using the Discovery DSC-C18 SPE column. The peptides were vacuum concentrated and dissolved in 25 µl of 3% acetonitrile containing 0.1% TFA, following spike-in with 200 pg of heavy isotope-labeled peptide (YI(¹³C,¹⁵N)MSDSNYV). The peptide solution (5 µl) was analyzed using an EASY-nLC 1000 system (Thermo Fisher Scientific) connected to a Q Exactive HF mass spectrometer (Thermo Electron) equipped with a nano-electrospray ion source. For liquid chromatography separation, an EASY-Spray ES902 column (C18, 2-µm beads, 100 Å, 75-µm inner diameter) capillary with a bed length of 25 cm was used. A flow rate of 300 nL min⁻¹ was employed with a solvent gradient of 7–35% B in 55 min to 90% B in 3 min. Solvent A was 0.1% formic acid, and solvent B was 0.1% formic acid–90% acetonitrile. The mass spectrometer was operated in parallel reaction-monitoring mode to specifically target the presence of endogenous FLT3 mutant (*m/z* = 1,091.4738¹⁺) and spiked-in isotope-labeled peptide (*m/z* = 1,098.4928¹⁺), eluting within a retention time window of 27–31 min, as determined using a synthetic analog. The MS/MS spectra using higher-energy collision-induced dissociation were acquired with a resolution of *R* = 15,000 after accumulation to a target of 1×10^5 . The normalized collision energy was set to NCE 27, and the isolation window was *m/z* = 2.0. The maximum allowed ion accumulation for the MS/MS spectrum was 120 ms. Raw data were analyzed using Xcalibur software and Skyline (MacCoss Lab Software).

pMHC-stability assay

HLA-A2 molecules were prepared in house, as previously described^{71,75,76}. The pMHC-stability assay was performed as previously described³⁸ with minor modifications. UV-mediated peptide-exchange reactions were performed for 1 h, followed by incubation of the resulting product at 4 °C. The next day, streptavidin-coated beads were washed twice with PBS–1% Tween. The peptide–HLA monomers were coupled with the washed beads for 10 min at room temperature. After coupling, the beads were washed twice with PBS–1% Tween and resuspended in 200 µl. An aliquot of 20 µl beads was set aside for the 0-h time point, while the remaining beads were incubated at 37 °C. Twenty microliters of beads were collected at 3, 6, 12 and 24 h of incubation. After collecting at each time point, the beads were stained with 30 µl of anti-HLA-A2–PE antibody (343305, BioLegend, 1:100 dilution) for 10 min at room temperature. Samples from all time points were analyzed immediately after staining on a BD LSR II Flow Cytometer.

Antibodies, dyes and flow cytometry

For surface antibody staining of human PB and BM cells, antibodies were added to cells for 15–20 min at 4 °C, followed by washing steps. For intracellular staining, cells were suspended in Cytofix/Cytoperm (BD Biosciences) solution for 20 min, washed with Perm/Wash buffer (BD Biosciences) and then stained with antibodies. For mouse PB, BM and spleen, cells were processed into a single-cell suspension as

previously described⁷⁷ and Fc receptor blocked (human, Miltenyi Biotech; mouse, produced by mouse hybridoma cell line clone 2.4 G2, ATCC, HB-197) for 10 min at 4 °C before staining with antibodies for 15–20 min at 4 °C. All fluorescently conjugated antibodies are described in Supplementary Table 10 and the Nature Portfolio Reporting Summary. In PDX mice, the percentage of myeloid cells was determined as a fraction of combined mouse and human leukocytes (mCD45⁺hCD45⁺), subtracting hCD3⁺ events accounting for infused T cells. Flow cytometry analysis was performed on the BD LSRII flow cytometer or the BD LSRFortessa machine (both BD Biosciences), while cell sorting was performed on the FACSAria Fusion cell sorter (BD Biosciences). Data were analyzed using FlowJo (TreeStar) or FACSDiva (BD Biosciences) software. To visually display flow cytometry data, we used an unsupervised nonlinear dimensionality-reduction algorithm such as t-SNE by using FlowJo (TreeStar) software.

T cell-activation assays

T cells transduced to express TCR were co-cultured with cell lines or primary patient tumor cells at an E:T cell ratio of 1:2 (100,000:200,000 cells per well), and reactivity was investigated by measuring CD137 upregulation or IFN-γ release. When indicated, target cells were pulsed with FLT3^{D/Y} or FLT3^{WT} peptide (purities >90%) or 161 single-amino acid-substituted variants of the FLT3^{D/Y} peptide (purity >70%) (GenScript Biotech) for 1–2 h or electroporated with mRNA encoding either FLT3^{WT} or the FLT3^{D/Y} minigene. Cells were placed in round- or flat-bottom 96-well plates and, after 18–20 h of co-incubation, were centrifuged at 700g for 2 min. Supernatants were collected for measurement of IFN-γ levels by ELISA, while cells were washed and stained with anti-CD137 antibody. In some experiments, transduced T cells were labeled with 0.75 µM CTV to distinguish them from target cells. Reagents for the IFN-γ ELISA were acquired from BD Pharmingen or R&D Systems: mouse anti-human IFN-γ capture antibody (NIB42), Biotin Mouse Anti-Human IFN-γ-detection antibody (4S.B3), streptavidin–HRP, stabilized tetramethylbenzidine and hydrogen peroxide as substrate solutions, sulfuric acid as the stop solution and recombinant human IFN-γ protein as the standard. The assay was performed according to the manufacturer's instructions.

Flow cytometry-based cytotoxicity assay using cell lines as targets

Transduced cell lines stably expressing the FLT3^{D/Y} minigene were co-cultured with CTV-labeled T cells transduced to express TCR at an E:T cell ratio of 1:2 (75,000:150,000 cells per well) for 48 h in round-bottom 96-well plates in triplicates. Following co-culture, cells were collected, washed and stained with human anti-CD3, anti-CD8 and anti-CD4 antibodies and LIVE/DEAD NIR for 15–20 min. Cells were then washed and resuspended in FACS buffer containing 10,000 Count-Bright Absolute Counting Beads (Thermo Fisher). An equal number of bead events (3,500) were recorded from every well. Normalized data were reported as percentage of the mean of the number of viable tumor cells acquired from three parallel wells co-cultured with TCR^{IG4} or TCR^{FLT3D/Y} cells from each donor.

Flow cytometry-based assays for T cell activation and cytotoxicity using primary human samples

PB or BM samples from patients were thawed and resuspended in IMDM with 20% (vol/vol) FCS (Trina biotech) and 0.1 mg ml⁻¹ DNase. Cells were centrifuged at 200g for 15 min at room temperature and transferred to round-bottom 96-well plates for assays measuring CD137 upregulation on T cells transduced to express TCR or cytotoxicity on target cells. Normal CD19⁺ B cells were isolated from healthy donor buffy coat MNCs using CD19-reactive microbeads and the autoMACS Pro Separator (Miltenyi Biotech) and transferred to round-bottom 96-well plates for assays measuring cytotoxicity on target cells. Individualized antibody panels and gating strategies to identify malignant blasts

and normal leukocyte populations were designed after reviewing diagnostic phenotyping available in the hospital records. Allogeneic or, for patients 1–3, also autologous patient-derived T cells transduced to express TCRs, were used in the experiments. Cells transduced to express TCR were prelabeled with CTV dye to distinguish them from target cells. For cytotoxicity assays, 75,000 T cells per well were co-incubated with 150,000 target cells in three parallel wells per condition for 72 h and then stained with individualized antibody panels for flow cytometry. CountBright Absolute Counting Beads were used as described above. Examples of the gating strategy used to identify live tumor cells in patients are shown in Extended Data Fig. 6a. For patients 1–6 and 8, myeloid cells were identified as CD3⁻CD19⁻CD20⁻, normal T cells as CD3⁺ and normal B cells as CD19⁺CD20⁺. Cells from patient 7 were obtained from Jackson Laboratory (stock ID J000106565), and the patient-specific phenotypic markers CD33 and CD19 were used to identify leukemia cells based on the characterization profile from the provider.

TCR^{FLT3D/Y} cell activity in the xenograft leukemia cell line model

This study was approved by the Norwegian Food Safety Authority (application ID 17500) and performed in compliance with institutional guidelines and the 2010/63/EU directive. Mice were observed for clinical signs of tumor spreading and were killed if they developed >20% weight loss, hunched posture, ruffled fur, limb paralysis or enlarged spleens. Maximum tumor burden was not exceeded. Experiments were terminated 2 months after T cell injection to avoid graft-versus-host disease, and surviving mice were killed humanely by cervical dislocation. Six mice were housed per cage in Eurostandard Type III cages (macrolone) with a light cycle from 7 a.m. to 7 p.m. at 22 ± 1 °C with 62 ± 5% humidity. Female (8–10-week-old) NSG (Jackson Laboratory) mice, bred in house, were sublethally irradiated (2.5 Gy, MultiRad225 X-ray, RPS Services) on day −15, and 4 × 10⁶ cells of the human B-ALL cell line BV173^{D835Y} were injected on day −14 through the tail vein. After leukemia was confirmed by BLI on day −1, mice were treated with 10⁷ T cells transduced to express TCR^{IG4} or TCR^{FLT3D/Y}. A group of control mice did not receive T cell injections. All mice were injected intraperitoneally (i.p.) daily with 2,500 IU IL-2 (R&D Systems). BLI imaging (by the IVIS Spectrum in vivo imaging system; analysis with Living Image software version 4.5.2, PerkinElmer) and blood analysis by flow cytometry were performed continuously. BM was collected at the endpoint and processed for flow cytometry to analyze the presence of T cells and tumor cells.

Activity of TCR^{FLT3D/Y} cells in four primary AML PDX models

Experiments were approved by Stockholms Djurförsöksetiska nämnd (17978-2018). The maximal tumor burden permitted was defined by the impact on the animal's health. Mice engrafted with leukemic cells were continuously monitored according to Karolinska Institutet's health assessment, and no animal exceeded the humane endpoint. The housing conditions were 21 °C and 45–50% humidity. Two to five mice were housed per cage in IVC-Mouse GM500 cages with a light cycle from 4 a.m. to 4 p.m. (patient 7) or from 6 a.m. to 6 p.m. (patient 1). BM was collected from femur, tibia and crista from both hind legs at terminal analysis. Mainly female mice were used in this study, but, when both sexes were used, they were equally distributed within the treatment groups. No sex-based analysis was thus performed.

Model 1. Female NOD.Cg-*Prkdc*^{scid} *Il2rg*^{tm1Wjl} Tg(CMV IL3,CSF2,KITLG)1Eav/MloySzJ (NSG-SGM3) mice stably engrafted with FLT3^{D835Y}-expressing HLA-A2⁺ AML cells from patient 7 (Supplementary Table 2 and 3) at 5 weeks of age were obtained from Jackson Laboratory (stock ID J000106565). Upon arrival (5.5 weeks after transplantation), PB myeloid engraftment was confirmed by flow cytometry, and mice were allocated to treatment groups (TCR^{FLT3D/Y} or TCR^{IG4} cells), resulting in a similar mean human myeloid engraftment

between the groups before infusion with T cells. Cryopreserved T cells transduced to express TCR were thawed and cultured in X-VIVO 20 medium (Lonza) with 5% HS, 1% penicillin–streptavidin and 5 ng ml⁻¹ IL-7 and IL-15 for 3–4 d before treatment. T cells containing 5 × 10⁶ CD8⁺mTCR-β⁺ T cells were injected through the lateral tail vein, and all mice received daily i.p. injections of 2,500 IU human IL-2 (R&D Systems). At day 8 after T cell infusion, half of the mice received a second dose of 5 × 10⁶ CD4-depleted (Miltenyi Biotec) TCR^{FLT3D/Y} or TCR^{IG4} T cells. As no differences were observed between the mice receiving one or two doses of T cells, the data from these mice were pooled. The effect of the T cells was monitored in serially collected PB and at termination 15 d after T cell treatment in the BM and spleen through detailed flow cytometry analysis.

Model 2. BM CD34⁺ cells from patient 1 (FLT3^{D/Y} and HLA-A2⁺; Supplementary Tables 2 and 3) were obtained by CD34 magnetic bead enrichment (Miltenyi Biotec) according to the manufacturer's instructions and as previously described⁷⁸. A total of 3 × 10⁵ CD34⁺ cells per mouse were intrafemorally injected into sublethally irradiated (3.3 Gy, X-ray source) female and male NSG-SGM3 mice (Jackson Laboratory, stock 013062) 9 weeks of age. Upon confirmation of stable PB myeloid engraftment 7 weeks after transplantation, mice were allocated to treatment groups (TCR^{FLT3D/Y} or TCR^{IG4} cells) based on their engraftment levels as described for patient 7. T cells containing 5 × 10⁶ CD8⁺mTCR-β⁺ T cells were infused into each mouse by lateral tail vein injections, and all mice received daily i.p. injections of 2,500 IU human IL-2 for 2 weeks, followed by less frequent injections. Mice were monitored using serially collected PB and at termination 34 d after T cell treatment with the BM and spleen.

Model 3. To mimic an MRD setting, secondary intrafemoral transplantation of BM cells from NSG mice (Jackson Laboratory, stock 005557) engrafted with material from patient 1 was performed into sublethally irradiated (2.5 Gy, X-ray source) female NSG mice 12–13 weeks of age. Following confirmation of low but stable leukemic engraftment 20 weeks after transplantation, mice were treated with TCR^{FLT3D/Y} or TCR^{IG4} CD4-depleted (Miltenyi Biotec) T cells (10 × 10⁶ T cells, containing 90% CD8⁺ and 10% CD4⁺ T cells). All mice were injected i.p. daily with 2,500 IU human IL-2. The effect of the T cells was evaluated in the BM 11 d after T cell treatment.

Model 4. Following secondary transplantation of BM from mice engrafted with patient 1 cells, BM from three NOD.Cg-*Prkdc*^{scid} *Il2rg*^{tm1Sug} Tg(CMV-IL2)4-2Jic/JicTac (NOG-HIL2, Taconic) mice was isolated and cultured for 48 h in CellGro GMP DC medium with 5% HS, IL-7 and IL-15 either with no T cells or with TCR^{IG4} or TCR^{FLT3D/Y} cells (E:T cell ratio, 1:2). After 48 h, the contents of each well were collected and intrafemorally injected into sublethally irradiated (2.25–2.5 Gy) female NSG mice 8–13 weeks of age. Engraftment levels were monitored in serially collected PB samples by flow cytometry. Data were pooled from two individual experiments. Differences in engraftment dynamics between mice engrafted with AML cells precultured with TCR^{FLT3D/Y} or TCR^{IG4} cells or without T cells was assessed by multilevel linear regression using the R package 'lmerTest'. Sampling time points and groups are treated as an interaction term with random effects for individual mice. Because the engraftment at the first time point was 0 for all mice except one, we fixed the intercept as 0. Estimated marginal means of models were obtained and compared between three groups using the R package 'emmeans'. Multiple tests were corrected using the Benjamini–Hochberg method. Only mice that could be followed until the end of the experiment were included in the analysis.

Whole-exome sequencing of cells from patient 1 and PDX mice
DNA was isolated from AML cells purified with the FACS Aria Fusion cell sorter (BD Biosciences) from patient 1 using the Maxwell RSC Cultured

Cells DNA Kit (Promega), including primary BM AML blasts ($CD3^-CD19^-$) and T cells ($CD3^+CD8^+CD19^-CD33^-$ and $CD3^+CD4^+CD19^-CD33^-$) and BM mCD45 $^-$ hCD45 $^+$ CD3 $^-$ CD19 $^-$ cells from one untreated and one TCR IG4 -treated PDX mouse from model 2. Whole-exome sequencing libraries were prepared with the Lotus DNA Library Prep Kit (IDT). Exon regions were captured using xGen Exome Hyb Panel v2 and the xGen Hybridization and Wash Kit (IDT) on 4 July 2022 and 5 July 2022. After mixing with 1% PhiX, prepared libraries were sequenced using the NextSeq high-output kit (300 cycles) with settings 'Read1, 151; Index1, 8; Index2, 8; Read2, 151'. Reads were aligned to the human (GRCh37) genome reference using Burrows–Wheeler Aligner version 0.7.17 with default parameter settings. PCR duplicates were marked with biobambam version 2.0.87. Reads were subjected to indel realignment and base quality score recalibration using GATK3 (version 3.8) and recalculation of MD/NM tags using SAMtools version 1.9. Errors associated with enzymatic fragmentation during library preparation were removed using FADE version 0.5.5, resulting in an average depth of 364 (331–439) in the final bam files⁷⁹.

Mutations calling was performed using GenomonFisher (<https://github.com/Genomon-Project/GenomonFisher>) with the following parameters: (1) mapping quality score ≥ 20 , (2) base quality score ≥ 15 , (3) number of total reads ≥ 8 , (4) number of variant reads ≥ 5 , (5) VAF ≥ 0.05 , (6) VAF in paired T cells < 0.1 , (7) VAF in other non-paired normal controls < 0.05 in all and average < 0.01 , (8) strand ratio in tumor $\neq 0$ or 1, (9) VAF by base counts divided by VAF by read count ≥ 0.5 and ≤ 2 , (10) P value by Fisher < 0.1 , (11) P value by EBFILTER⁸⁰ < 0.001 , (12) mutation on exons, (13) not on the repeat regions.

Mutations were annotated by ANNOVAR⁸¹. Copy number analysis was performed using CNACS⁸². The WT1 H507P mutation was, together with the FLT3 D835Y mutation, the only identified potential driver mutation in AML^{15,83}.

Droplet digital PCR

ddPCR was performed to quantify clonal involvement. DNA from patient 1 with AML was isolated as explained above, and DNA from AML PDX mice was isolated through flow cytometry sorting of mCD45 $^-$ mTer119 $^-$ hCD45 $^+$ CD3 $^-$ cells (PDX patient 7) or hCD45 $^+$ CD33 $^+$ CD34 $^+$, hCD45 $^+$ CD33 $^+$ CD34 $^+$ and hCD45 $^+$ CD19 $^+$ cells (PDX patient 1) and subjected to whole-genome DNA amplification using the REPLI-g Single Cell Kit (QIAGEN) according to the manufacturer's instructions. Samples with < 90 cells were excluded. Briefly, a 20- μ l PCR reaction mixture containing 1× ddPCR supermix for probes (no dUTP) (Bio-Rad), 1× primer-probe assay (FLT3 D835Y , dHsaMDV2010047; WT1 H507P , dHsaMDS871718945; Bio-Rad) and 60 ng DNA was mixed with Droplet Generation Oil for Probes (Bio-Rad). Droplets were prepared according to the manufacturer's instructions on a QX200 droplet generator (Bio-Rad) and subjected to PCR (Bio-Rad): 95 °C for 10 min, 40 cycles of 94 °C for 30 s and 55 °C for 60 s and a 10-min incubation at 98 °C. Plates were read on a QX200 droplet reader (Bio-Rad) and analyzed using QuantaSoft version 1.5.38.1118 software (Bio-Rad) to calculate VAFs and 95% confidential intervals. The numbers of FLT3 D835Y cells in the AML PDX mice were determined by combining the information from the fraction of mutated cells identified by ddPCR, and the frequency of phenotypically defined subsets (hCD45 $^+$ CD3 $^-$ or hCD45 $^+$ CD33 $^+$ CD34 $^-$ and hCD45 $^+$ CD33 $^+$ CD34 $^+$, respectively, for patients 7 and 1) in the BM as determined by flow cytometry, and the total number of MNCs in the BM was counted with Sysmex.

External AML-targeted sequencing data analysis

Mutation data (SNVs and indels) from AML patients reported by Papaemmanuil et al.¹⁵ were downloaded from <https://www.cbioportal.org>. VAF was estimated from reported alternative allele reads divided by sequencing depth for the position. Patients harboring a FLT3 D835Y mutation were selected for in-depth analysis.

The order of FLT3 mutations in AML using VAF and the mutated cell fraction was determined from the publicly available mutation list identified by targeted DNA sequencing by Morita et al.⁴⁵.

Statistical analysis and reproducibility

Statistical analysis was performed in GraphPad Prism versions 6–8 (GraphPad Software). Comparison of mean values between two experimental groups was conducted with unpaired, two-tailed Student's test. The ordinary ANOVA test with adjustment for multiple comparisons with Tukey's post hoc test was employed for comparisons of more than two experimental groups. To determine differences between *in vivo* treatment groups in the PDX mouse models, Kruskal–Wallis ANOVA with Dunn's multiple-comparison test and two-tailed Mann–Whitney test were performed. P values < 0.05 were considered statistically significant. The investigators were not blinded to allocation during experiments or to outcome assessment. PDX models 1–3 were performed once each, and data for PDX model 4 were generated from two independent experiments with mice from all treatment groups represented in both experiments. No statistical method was used to predetermine sample size, and experiments were not randomized. Sample sizes were estimated based on preliminary experiments and are similar to those previously reported^{27,84}. Due to the nature of the other *in vitro* experiments, blinding was not possible and is not generally performed in the field as the data acquisition is quantitative (flow cytometry or MS) rather than qualitative and therefore less influenced by observer bias. Data distribution was assumed to be normal, but this was not formally tested. Data distribution is shown as individual data points.

Illustrations

Fig. 1a was generated by Science Shaped (<https://scienceshaped.com/>). All mouse illustrations were generated using Adobe Illustrator 2022 version 26.0.3.

Reporting summary

Further information on research design is available in the Nature Portfolio Reporting Summary linked to this article.

Data availability

The data that support the findings of this study are included in the text and in the Supplementary Information. Additional datasets used in the study are: the UniProt *Homo sapiens* database, using Mascot version 2.2.07 (<https://www.matrixscience.com>), curated human proteome databases UniProtKB/Swiss-Prot and the Protein Data Bank using the ScanProsite tool (<https://prosite.expasy.org/scanprosite/>), the pMHC class I binding prediction algorithm NetMHC version 4.0 (<http://www.cbs.dtu.dk/services/NetMHC/>), data from Papaemmanuil et al.¹⁵ (<https://www.cbioportal.org>) and data from Morita et al.⁴⁵. Exome sequencing data have been deposited at the European Genome–Phenome Archive, which is hosted by the EBI and the CRG, under accession number EGAS00001007467 and can be shared according to institutional guidelines at Oslo University Hospital upon reasonable request. Mass spectrometry data have been deposited at the Proteomics Identification Database under accession number PXD043908. All other data supporting the findings of this study are available from the corresponding author on reasonable request. Source data are provided with this paper.

References

- Coulie, P. G. et al. A mutated intron sequence codes for an antigenic peptide recognized by cytolytic T lymphocytes on a human melanoma. *Proc. Natl Acad. Sci. USA* **92**, 7976–7980 (1995).
- Wolfel, T. et al. A p16INK4a-insensitive CDK4 mutant targeted by cytolytic T lymphocytes in a human melanoma. *Science* **269**, 1281–1284 (1995).

3. Matsushita, H. et al. Cancer exome analysis reveals a T-cell-dependent mechanism of cancer immunoediting. *Nature* **482**, 400–404 (2012).
4. Castle, J. C. et al. Exploiting the mutanome for tumor vaccination. *Cancer Res.* **72**, 1081–1091 (2012).
5. van Rooij, N. et al. Tumor exome analysis reveals neoantigen-specific T-cell reactivity in an ipilimumab-responsive melanoma. *J. Clin. Oncol.* **31**, e439–e442 (2013).
6. Rizvi, N. A. et al. Cancer immunology. Mutational landscape determines sensitivity to PD-1 blockade in non-small cell lung cancer. *Science* **348**, 124–128 (2015).
7. Yarchoan, M., Hopkins, A. & Jaffee, E. M. Tumor mutational burden and response rate to PD-1 inhibition. *N. Engl. J. Med.* **377**, 2500–2501 (2017).
8. Tran, E. et al. Cancer immunotherapy based on mutation-specific CD4⁺ T cells in a patient with epithelial cancer. *Science* **344**, 641–645 (2014).
9. Tran, E. et al. T-cell transfer therapy targeting mutant KRAS in cancer. *N. Engl. J. Med.* **375**, 2255–2262 (2016).
10. Zacharakis, N. et al. Immune recognition of somatic mutations leading to complete durable regression in metastatic breast cancer. *Nat. Med.* **24**, 724–730 (2018).
11. Karpanen, T. & Olweus, J. The potential of donor T-cell repertoires in neoantigen-targeted cancer immunotherapy. *Front. Immunol.* **8**, 1718 (2017).
12. Foy, S. P. et al. Non-viral precision T cell receptor replacement for personalized cell therapy. *Nature* **615**, 687–696 (2023).
13. Leidner, R. et al. Neoantigen T-cell receptor gene therapy in pancreatic cancer. *N. Engl. J. Med.* **386**, 2112–2119 (2022).
14. Kim, S. P. et al. Adoptive cellular therapy with autologous tumor-infiltrating lymphocytes and T-cell receptor-engineered T cells targeting common p53 neoantigens in human solid tumors. *Cancer Immunol. Res.* **10**, 932–946 (2022).
15. Papaemmanuil, E. et al. Genomic classification and prognosis in acute myeloid leukemia. *N. Engl. J. Med.* **374**, 2209–2221 (2016).
16. Socie, G. & Blazar, B. R. Acute graft-versus-host disease: from the bench to the bedside. *Blood* **114**, 4327–4336 (2009).
17. Mardiana, S. & Gill, S. CAR T cells for acute myeloid leukemia: state of the art and future directions. *Front. Oncol.* **10**, 697 (2020).
18. Daver, N., Alotaibi, A. S., Bucklein, V. & Subklewe, M. T-cell-based immunotherapy of acute myeloid leukemia: current concepts and future developments. *Leukemia* **35**, 1843–1863 (2021).
19. Kenderian, S. S. et al. CD33-specific chimeric antigen receptor T cells exhibit potent preclinical activity against human acute myeloid leukemia. *Leukemia* **29**, 1637–1647 (2015).
20. Gill, S. et al. Preclinical targeting of human acute myeloid leukemia and myeloablation using chimeric antigen receptor-modified T cells. *Blood* **123**, 2343–2354 (2014).
21. Jetani, H. et al. CAR T-cells targeting FLT3 have potent activity against FLT3^{ITD} AML and act synergistically with the FLT3-inhibitor crenolanib. *Leukemia* **32**, 1168–1179 (2018).
22. Olweus, J. et al. Dendritic cell ontogeny: a human dendritic cell lineage of myeloid origin. *Proc. Natl Acad. Sci. USA* **94**, 12551–12556 (1997).
23. Kim, M. Y. et al. Genetic inactivation of CD33 in hematopoietic stem cells to enable CAR T cell immunotherapy for acute myeloid leukemia. *Cell* **173**, 1439–1453 (2018).
24. Haubner, S. et al. Coexpression profile of leukemic stem cell markers for combinatorial targeted therapy in AML. *Leukemia* **33**, 64–74 (2019).
25. Tambaro, F. P. et al. Autologous CD33-CAR-T cells for treatment of relapsed/refractory acute myelogenous leukemia. *Leukemia* **35**, 3282–3286 (2021).
26. Laszlo, G. S., Estey, E. H. & Walter, R. B. The past and future of CD33 as therapeutic target in acute myeloid leukemia. *Blood Rev.* **28**, 143–153 (2014).
27. Ali, M. et al. T cells targeted to TdT kill leukemic lymphoblasts while sparing normal lymphocytes. *Nat. Biotechnol.* **40**, 488–498 (2021).
28. Chapuis, A. G. et al. T cell receptor gene therapy targeting WT1 prevents acute myeloid leukemia relapse post-transplant. *Nat. Med.* **25**, 1064–1072 (2019).
29. van der Lee, D. I. et al. Mutated nucleophosmin 1 as immunotherapy target in acute myeloid leukemia. *J. Clin. Invest.* **129**, 774–785 (2019).
30. Xie, G. et al. CAR-T cells targeting a nucleophosmin neoepitope exhibit potent specific activity in mouse models of acute myeloid leukaemia. *Nat. Biomed. Eng.* **5**, 399–413 (2021).
31. Biernacki, M. A. et al. CBFB-MYH11 fusion neoantigen enables T cell recognition and killing of acute myeloid leukemia. *J. Clin. Invest.* **130**, 5127–5141 (2020).
32. Daver, N., Schlenk, R. F., Russell, N. H. & Levis, M. J. Targeting FLT3 mutations in AML: review of current knowledge and evidence. *Leukemia* **33**, 299–312 (2019).
33. Daver, N. et al. Secondary mutations as mediators of resistance to targeted therapy in leukemia. *Blood* **125**, 3236–3245 (2015).
34. Stone, R. M. et al. Midostaurin plus chemotherapy for acute myeloid leukemia with a FLT3 mutation. *N. Engl. J. Med.* **377**, 454–464 (2017).
35. Smith, C. C. et al. Validation of ITD mutations in FLT3 as a therapeutic target in human acute myeloid leukaemia. *Nature* **485**, 260–263 (2012).
36. Smith, C. C., Lin, K., Stecula, A., Sali, A. & Shah, N. P. FLT3 D835 mutations confer differential resistance to type II FLT3 inhibitors. *Leukemia* **29**, 2390–2392 (2015).
37. Smith, C. C. et al. Heterogeneous resistance to quizartinib in acute myeloid leukemia revealed by single-cell analysis. *Blood* **130**, 48–58 (2017).
38. Stronen, E. et al. Targeting of cancer neoantigens with donor-derived T cell receptor repertoires. *Science* **352**, 1337–1341 (2016).
39. Ali, M. et al. Induction of neoantigen-reactive T cells from healthy donors. *Nat. Protoc.* **14**, 1926–1943 (2019).
40. Cohen, C. J., Zhao, Y., Zheng, Z., Rosenberg, S. A. & Morgan, R. A. Enhanced antitumor activity of murine–human hybrid T-cell receptor (TCR) in human lymphocytes is associated with improved pairing and TCR/CD3 stability. *Cancer Res.* **66**, 8878–8886 (2006).
41. Robbins, P. F. et al. Tumor regression in patients with metastatic synovial cell sarcoma and melanoma using genetically engineered lymphocytes reactive with NY-ESO-1. *J. Clin. Oncol.* **29**, 917–924 (2011).
42. Bethune, M. T. et al. Isolation and characterization of NY-ESO-1-specific T cell receptors restricted on various MHC molecules. *Proc. Natl Acad. Sci. USA* **115**, E10702–E10711 (2018).
43. Marcu, A. et al. HLA Ligand Atlas: a benign reference of HLA-presented peptides to improve T-cell-based cancer immunotherapy. *J. Immunother. Cancer* **9**, e002071 (2021).
44. Jaiswal, S. & Ebert, B. L. Clonal hematopoiesis in human aging and disease. *Science* **366**, eaan4673 (2019).
45. Morita, K. et al. Clonal evolution of acute myeloid leukemia revealed by high-throughput single-cell genomics. *Nat. Commun.* **11**, 5327 (2020).
46. Shlush, L. I. et al. Identification of pre-leukaemic haematopoietic stem cells in acute leukaemia. *Nature* **506**, 328–333 (2014).
47. Goardon, N. et al. Coexistence of LMP-like and GMP-like leukemia stem cells in acute myeloid leukemia. *Cancer Cell* **19**, 138–152 (2011).

48. Lapidot, T. et al. A cell initiating human acute myeloid leukaemia after transplantation into SCID mice. *Nature* **367**, 645–648 (1994).
49. Bonnet, D. & Dick, J. E. Human acute myeloid leukemia is organized as a hierarchy that originates from a primitive hematopoietic cell. *Nat. Med.* **3**, 730–737 (1997).
50. Schuurhuis, G. J. et al. Minimal/measurable residual disease in AML: a consensus document from the European LeukemiaNet MRD Working Party. *Blood* **131**, 1275–1291 (2018).
51. Pearlman, A. H. et al. Targeting public neoantigens for cancer immunotherapy. *Nat. Cancer* **2**, 487–497 (2021).
52. Bassani-Sternberg, M. & Coukos, G. Mass spectrometry-based antigen discovery for cancer immunotherapy. *Curr. Opin. Immunol.* **41**, 9–17 (2016).
53. Loffler, M. W. et al. Multi-omics discovery of exome-derived neoantigens in hepatocellular carcinoma. *Genome Med.* **11**, 28 (2019).
54. Sykulev, Y., Joo, M., Vturina, I., Tsomides, T. J. & Eisen, H. N. Evidence that a single peptide–MHC complex on a target cell can elicit a cytolytic T cell response. *Immunity* **4**, 565–571 (1996).
55. Scheper, W. et al. Low and variable tumor reactivity of the intra-tumoral TCR repertoire in human cancers. *Nat. Med.* **25**, 89–94 (2019).
56. Lowery, F. J. et al. Molecular signatures of antitumor neoantigen-reactive T cells from metastatic human cancers. *Science* **375**, 877–884 (2022).
57. Nagarsheth, N. B. et al. TCR-engineered T cells targeting E7 for patients with metastatic HPV-associated epithelial cancers. *Nat. Med.* **27**, 419–425 (2021).
58. Sahin, U. et al. Personalized RNA mutanome vaccines mobilize poly-specific therapeutic immunity against cancer. *Nature* **547**, 222–226 (2017).
59. Ott, P. A. et al. An immunogenic personal neoantigen vaccine for patients with melanoma. *Nature* **547**, 217–221 (2017).
60. Lang, F., Schrorts, B., Lower, M., Tureci, O. & Sahin, U. Identification of neoantigens for individualized therapeutic cancer vaccines. *Nat. Rev. Drug Discov.* **21**, 261–282 (2022).
61. Johnson, L. A. et al. Gene therapy with human and mouse T-cell receptors mediates cancer regression and targets normal tissues expressing cognate antigen. *Blood* **114**, 535–546 (2009).
62. Jin, B. Y. et al. Engineered T cells targeting E7 mediate regression of human papillomavirus cancers in a murine model. *JCI Insight* **3**, e99488 (2018).
63. Duan, F. et al. Genomic and bioinformatic profiling of mutational neoepitopes reveals new rules to predict anticancer immunogenicity. *J. Exp. Med.* **211**, 2231–2248 (2014).
64. Chandran, S. S. et al. Immunogenicity and therapeutic targeting of a public neoantigen derived from mutated PIK3CA. *Nat. Med.* **28**, 946–957 (2022).
65. Foldvari Z, Knetter C, Yang W, et al. A systematic safety pipeline for selection of T-cell receptors to enter clinical use. *NPJ Vaccines* <https://doi.org/10.1038/s41541-023-00713-y> (2023).
66. Jan, M. et al. Clonal evolution of preleukemic hematopoietic stem cells precedes human acute myeloid leukemia. *Sci. Transl. Med.* **4**, 149ra18 (2012).
67. Mansilla-Soto, J. et al. HLA-independent T cell receptors for targeting tumors with low antigen density. *Nat. Med.* **28**, 345–352 (2022).
68. Dolgin, E. First soluble TCR therapy opens ‘new universe’ of cancer targets. *Nat. Biotechnol.* **40**, 441–444 (2022).
69. Abrahamsen, I. W. et al. Targeting B cell leukemia with highly specific allogeneic T cells with a public recognition motif. *Leukemia* **24**, 1901–1909 (2010).
70. Kumari, S. et al. Alloreactive cytotoxic T cells provide means to decipher the immunoepitidome and reveal a plethora of tumor-associated self-epitopes. *Proc. Natl Acad. Sci. USA* **111**, 403–408 (2014).
71. Toebe, M. et al. Design and use of conditional MHC class I ligands. *Nat. Med.* **12**, 246–251 (2006).
72. Hadrup, S. R. et al. Parallel detection of antigen-specific T-cell responses by multidimensional encoding of MHC multimers. *Nat. Methods* **6**, 520–526 (2009).
73. Linnemann, C. et al. High-throughput identification of antigen-specific TCRs by TCR gene capture. *Nat. Med.* **19**, 1534–1541 (2013).
74. Brochet, X., Lefranc, M. P. & Giudicelli, V. IMGT/V-QUEST: the highly customized and integrated system for Ig and TR standardized V-J and V-D-J sequence analysis. *Nucleic Acids Res.* **36**, W503–W508 (2008).
75. Toebe, M., Rodenko, B., Ovaa, H. & Schumacher, T. N. Generation of peptide MHC class I monomers and multimers through ligand exchange. *Curr. Protoc. Immunol.* **87**, 18.16.1–18.16.20 (2009).
76. Sikorski, K. et al. A high-throughput pipeline for validation of antibodies. *Nat. Methods* **15**, 909–912 (2018).
77. Carrelha, J. et al. Hierarchically related lineage-restricted fates of multipotent haematopoietic stem cells. *Nature* **554**, 106–111 (2018).
78. Woll, P. S. et al. Myelodysplastic syndromes are propagated by rare and distinct human cancer stem cells in vivo. *Cancer Cell* **25**, 794–808 (2014).
79. Gregory, T. et al. Characterization and mitigation of fragmentation enzyme-induced dual stranded artifacts. *NAR Genom. Bioinform.* **2**, lqaa070 (2020).
80. Shiraishi, Y. et al. An empirical Bayesian framework for somatic mutation detection from cancer genome sequencing data. *Nucleic Acids Res.* **41**, e89 (2013).
81. Wang, K., Li, M. & Hakonarson, H. ANNOVAR: functional annotation of genetic variants from high-throughput sequencing data. *Nucleic Acids Res.* **38**, e164 (2010).
82. Yoshizato, T. et al. Genetic abnormalities in myelodysplasia and secondary acute myeloid leukemia: impact on outcome of stem cell transplantation. *Blood* **129**, 2347–2358 (2017).
83. Rampal, R. & Figueroa, M. E. Wilms tumor 1 mutations in the pathogenesis of acute myeloid leukemia. *Haematologica* **101**, 672–679 (2016).
84. Jain, N. et al. TET2 guards against unchecked BATF3-induced CAR T cell expansion. *Nature* **615**, 315–322 (2023).
85. Juritz, V. et al. NetMHCpan-4.0: improved peptide–MHC class I interaction predictions integrating eluted ligand and peptide binding affinity data. *J. Immunol.* **199**, 3360–3368 (2017).
86. Wang, M. et al. Validation of risk stratification models in acute myeloid leukemia using sequencing-based molecular profiling. *Leukemia* **31**, 2029–2036 (2017).

Acknowledgements

We thank the Oslo University Hospital (OUH) flow cytometry core facility for excellent technical assistance. This work was supported by the Research Council of Norway through its Centres of Excellence scheme (332727) and through grant 316060, the Norwegian Cancer Society grant 216135-2020, South-Eastern Regional Health Authority Norway (2021074), the Norwegian Childhood Cancer Foundation, Stiftelsen Kristian Gerhard Jebsen, the European Research Council under the European Union’s Horizon 2020 research and innovation program (grant agreement no. 865805), the University of Oslo and Oslo University Hospital and the Novo Nordisk Foundation (to J.O.), by the Knut and Alice Wallenberg Foundation (KAW 2016.0105 to S.E.W.J. and KAW 2015.0195 to P.S.W.), the Swedish Research Council (538-2013-8995 to S.E.W.J. and 2015-03561 to P.S.W.) and by funding to S.E.W.J.: the Tobias Foundation (4-1122/2014), the Torsten Söderberg Foundation, the Center for Innovative Medicine at Karolinska Institutet (613/06) and the UK Medical Research Council (MC_UU_12009/5).

Author contributions

E.G.: conceptualization, methodology, acquisition, analysis and interpretation of data, investigation, writing (original draft), writing (review and editing). M. Lehander and S.V.C.: methodology, acquisition, analysis and data interpretation, writing (original draft), writing (review and editing). W.Y., Y.L., T.K., M.M.N., R.C.B., T.T.T., T.Y., E.H.R., K.D., M. Laos, J.S.H., A.K.B., S.M., D.W.L.C.: acquisition, analysis and data interpretation. T.J.G., M.D.-S., A.H.: project administration, resources. M.A., A.M.: methodology. M.B., M.G., T.G.-D., S.L.: resources. S.E.W.J.: conceptualization, methodology, analysis and interpretation of data, investigation, supervision, funding acquisition, writing (original draft), writing (review and editing). P.S.W.: conceptualization, methodology, acquisition, analysis and interpretation of data, investigation, supervision, resources, writing (original draft), writing (review and editing). J.O.: conceptualization, methodology, supervision, analysis and interpretation of data, investigation, funding acquisition, writing (original draft), writing (review and editing).

Competing interests

A patent application has been filed by the Oslo University Hospital institutional technology transfer office Inven2 protecting the TCR sequence (J.O. and E.G. are inventors). J.O. is on the scientific advisory board of Asgard Therapeutics and is a cofounder of T-Rx therapeutics, a company that aims to develop TCR T cell therapies. The other co-authors declare no competing interests.

Additional information

Extended data is available for this paper at
<https://doi.org/10.1038/s43018-023-00642-8>.

Supplementary information The online version contains supplementary material available at <https://doi.org/10.1038/s43018-023-00642-8>.

Correspondence and requests for materials should be addressed to Sten Eirik W. Jacobsen, Petter S. Woll or Johanna Olweus.

Peer review information *Nature Cancer* thanks Saar Gill, Alexandre Harari and Claude Perreault for their contribution to the peer review of this work.

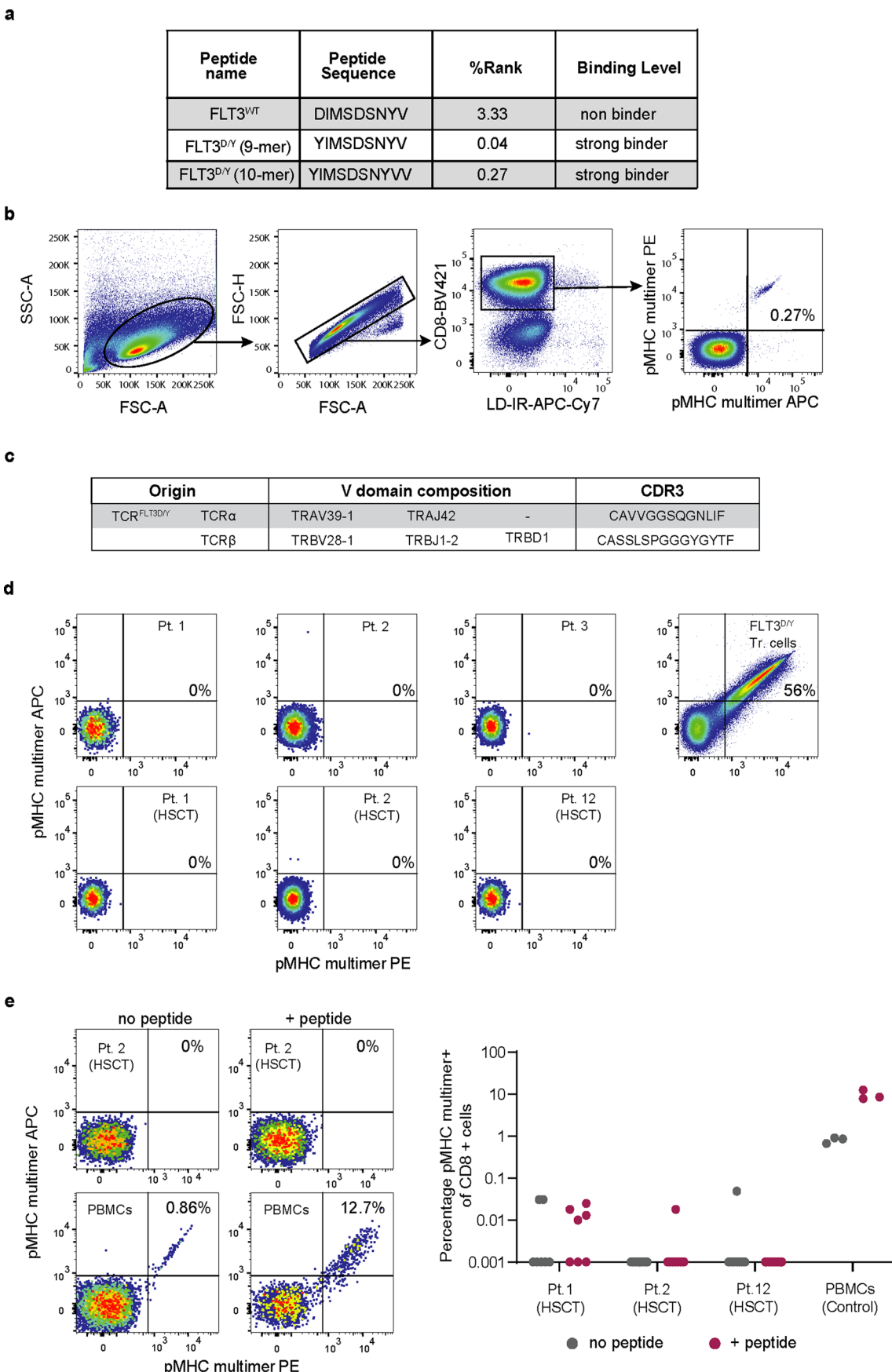
Reprints and permissions information is available at www.nature.com/reprints.

Publisher's note Springer Nature remains neutral with regard to jurisdictional claims in published maps and institutional affiliations.

Open Access This article is licensed under a Creative Commons Attribution 4.0 International License, which permits use, sharing, adaptation, distribution and reproduction in any medium or format, as long as you give appropriate credit to the original author(s) and the source, provide a link to the Creative Commons license, and indicate if changes were made. The images or other third party material in this article are included in the article's Creative Commons license, unless indicated otherwise in a credit line to the material. If material is not included in the article's Creative Commons license and your intended use is not permitted by statutory regulation or exceeds the permitted use, you will need to obtain permission directly from the copyright holder. To view a copy of this license, visit <http://creativecommons.org/licenses/by/4.0/>.

© The Author(s) 2023

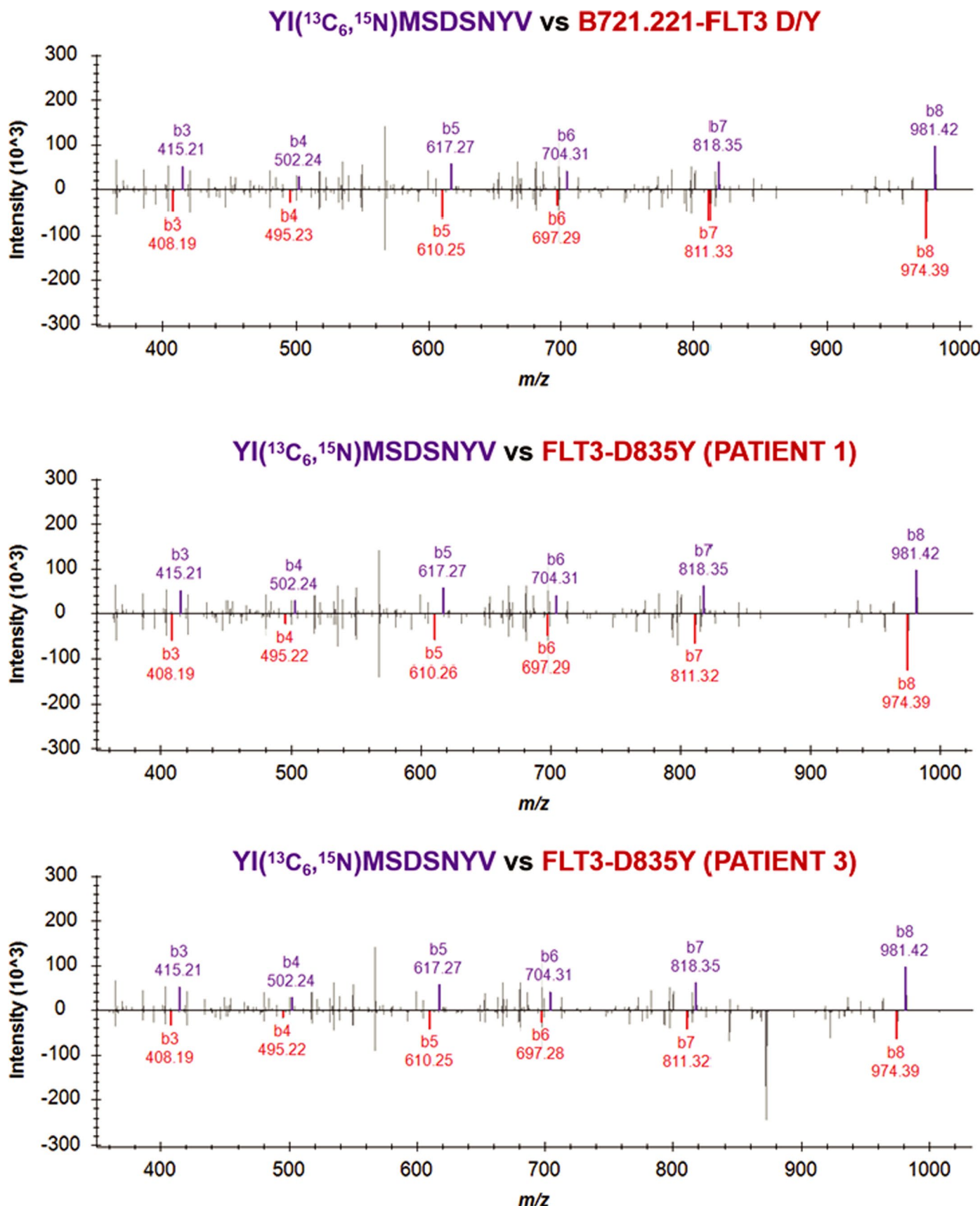
¹Department of Cancer Immunology, Oslo University Hospital Radiumhospitalet, Oslo, Norway. ²Institute of Clinical Medicine, University of Oslo, Oslo, Norway. ³Department of Medicine Huddinge, Center for Hematology and Regenerative Medicine, Karolinska Institutet, Stockholm, Sweden. ⁴Genomics Group, Faculty of Biosciences and Aquaculture, Nord University, Bodø, Norway. ⁵Department of Immunology, Oslo University Hospital, Oslo, Norway. ⁶Department of Cell and Molecular Biology, Karolinska Institutet, Stockholm, Sweden. ⁷Department of Immunology, University of Oslo and Oslo University Hospital, Oslo, Norway. ⁸Section for Experimental and Translational Immunology, Department of Health Technology, Technical University of Denmark, Kongens Lyngby, Denmark. ⁹Department of Hematology, Aarhus University Hospital, Aarhus, Denmark. ¹⁰Department of Hematology, Leiden University Medical Center, Leiden, the Netherlands. ¹¹Hematology Department, Section for Stem Cell Transplantation, Oslo University Hospital, Rikshospitalet, Clinic for Cancer Medicine, Oslo, Norway. ¹²Karolinska University Hospital, Stockholm, Sweden. ¹³Department of Medical Sciences, Uppsala University, Uppsala, Sweden. ¹⁴MRC Molecular Haematology Unit, MRC Weatherall Institute of Molecular Medicine, University of Oxford, Oxford, UK. ¹⁵These authors contributed equally: Sten Eirik W. Jacobsen, Petter S. Woll.  e-mail: sten.eirik.jacobsen@ki.se; petter.woll@ki.se; johanna.olweus@medisin.uio.no



Extended Data Fig. 1 | See next page for caption.

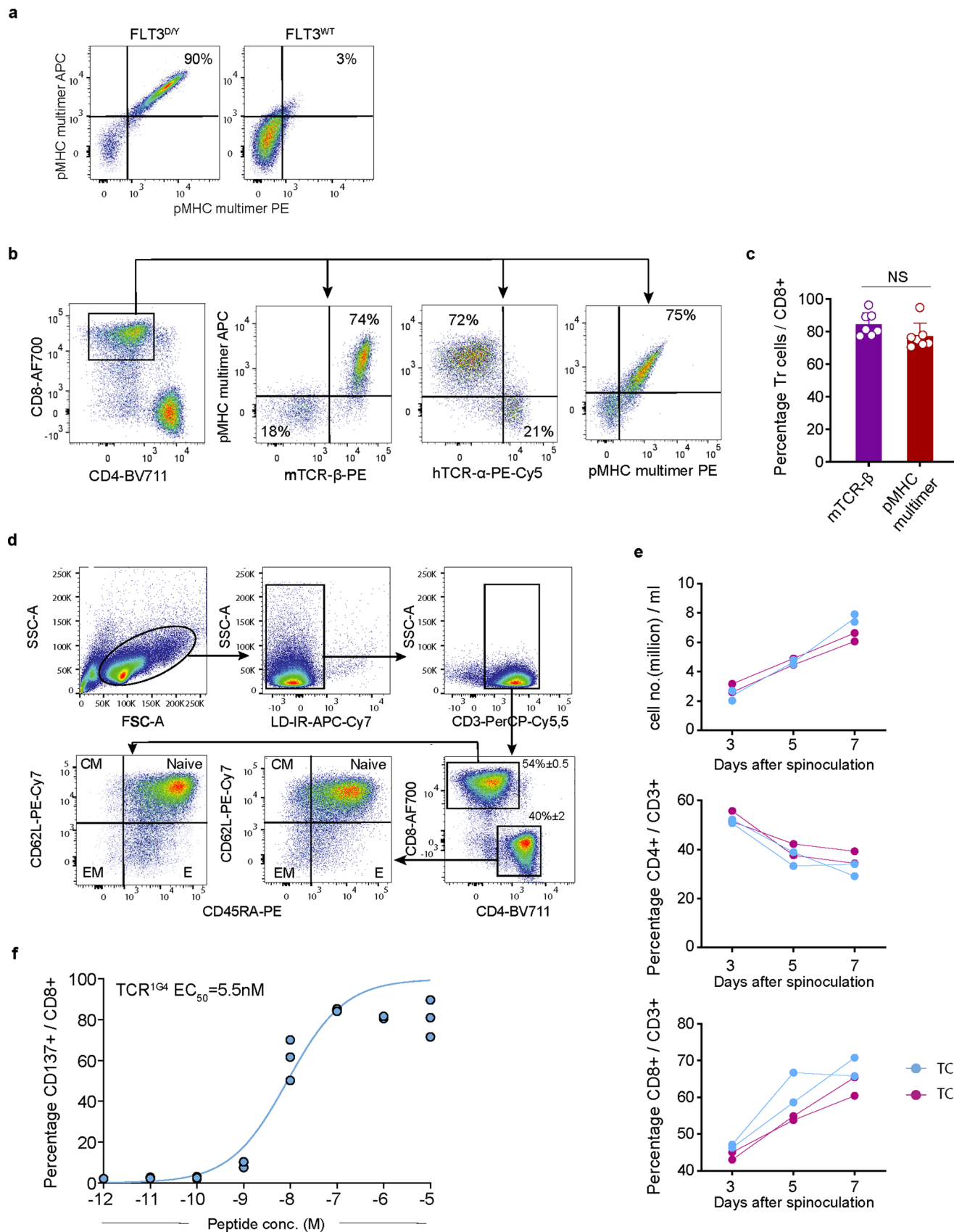
Extended Data Fig. 1 | T cells reactive to FLT3^{D/Y} HLA-A2 can be induced by culture of naïve healthy donor T cells but are not identified among memory T cells from AML patients in diagnostic samples or following HSCT. (a) Predicted binding affinity of FLT3^{D/Y} and FLT3^{WT} peptides using the NetMHC-4.0 algorithm. Peptides with affinity <50 nM (EL%Rank <0.500) classify as strong binders, 50 nM<affinity<500 nM (EL%Rank <2.000) as weak binders and affinity >500 nM as non- binders⁸⁵. (b) Gating strategy to identify CD8⁺ T cells staining as double positive events for pMHC multimers (APC- and PE-conjugated) complexed with the FLT3^{D/Y} peptide. The three left plots show gates used for FSC/SSC, singlets and Live/Dead Fixable Near-IR^{neg}/CD8⁺ events. The plot to the right shows multimer positive events in co-culture of naïve healthy donor CD8⁺ T cells with autologous moDCs transfected with target mRNA. (c) The

TCR^{FLT3D/Y} sequence. (d) Staining of samples from AML patients taken at point of diagnosis (top row, left three panels) and post allo-HSCT (bottom row) with pMHC multimers. TCR^{FLT3D/Y}* transduced T cells were used as a positive control for multimer staining (top right). (e) Staining of samples obtained from patient 2 after allo-HSCT following 5 days of *in vitro* expansion in absence (left) and presence (right) of the FLT3^{D/Y} peptide (top panels). As positive control for *in vitro* expansion of memory T cells, TCR^{FLT3D/Y} T cells were spiked into autologous healthy PBMCs under the same conditions (bottom panels). Inset numbers represent the percentage of pMHC multimer⁺ cells out of CD8⁺ cells. The graph to the right shows data for all three patients and positive controls. Data shown are from one experiment with each dot representing a technical replicate ($n = 7$ for pt 1, $n = 12$ for pt 2, $n = 8$ for pt 12 and $n = 3$ for PBMC healthy donor).



Extended Data Fig. 2 | Tandem mass spectra of endogenous vs isotopically labelled peptide. Mirror image plots comparing the fragmentation spectra of endogenous FLT3^{D/Y} peptide to its isotopically labelled counterpart YI(¹³C₆,¹⁵N)

MSDSNYV. Spectra obtained from immunoprecipitated HLA derived from the B721.221 cell line retrovirally transduced with a minigene encoding the D835Y mutation, and from patient 1 and patient 3, are displayed.

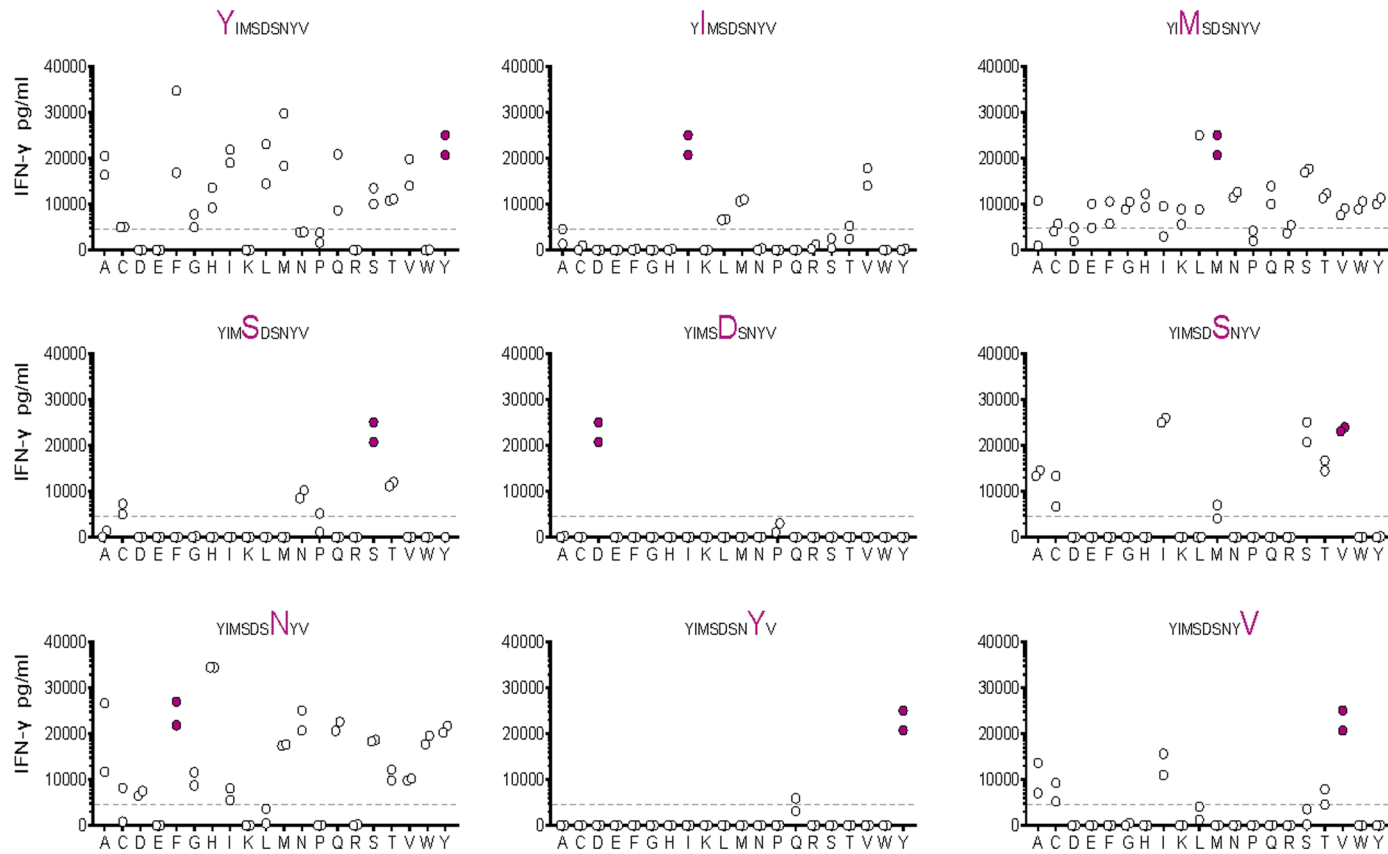


Extended Data Fig. 3 | See next page for caption.

Extended Data Fig. 3 | TCR^{FLT3D/Y} cells maintain a predominantly naïve phenotype following expansion. (a) Staining of TCR^{FLT3D/Y} cells with pMHC multimers complexed with either the FLT3^{D/Y} or the FLT3WT peptide (each multimer conjugated to both APC and PE, gating strategy shown in Extended Data Fig. 1b. Data shown is from one representative donor out of two stained in one experiment. (b) Gating strategy for TCR^{FLT3D/Y} cells. Panels show gating on: CD8⁺ cells labeled with the APC pMHC multimer and antibodies reactive to mouse TCR-β or human TCR-α (middle panels), and CD8⁺ cells staining positively for APC and PE-labeled pMHC multimers complexed with the FLT3^{D/Y} peptide (right plot). (c) Percentage of mTCR-β⁺ cells or pMHC multimer⁺ cells among CD8⁺ cells following transduction with the TCR^{FLT3D/Y}. Each data point represents a different HLA-A2^{pos} donor ($n = 7$ donors from 3 independent experiments). Data are analyzed by unpaired, two-tailed Student's t-test and $p < 0.05$ was considered statistically significant. (d) Gating strategy to identify differentiation stages of

TCR-transduced T cells three days after spinoculation. Top panels show gating on FSC/SSC^{hi}, Live/Dead Fixable Near-IR^{neg}, CD3⁺ events. Bottom panels show gating on CD4⁺ or CD8⁺ populations and subsequent identification of naïve, central memory (CM), effector (E) and effector memory (EM) cells as defined by expression of CD45RA and CD62L analyzed in two donors in one experiment. (e) Expansion of HLA-A2^{pos} PB T cells from two donors transduced in parallel with the TCR^{FLT3D/Y} or TCR^{IG4} following indicated days after retroviral transduction. Data are from one experiment and dots represent one technical replicate for each HLA-A2^{pos} PB T cell donor. (f) Activation of TCR^{IG4} cells measured as upregulation of $CD137$ after co-incubation with peptide-pulsed (NY-ESO-1 peptide SLLMWITQC) BV173 cells (K562 cells were not used, in contrast to Fig. 1f, as they express NY-ESO-1). EC₅₀ = half maximal effective concentration (linear curve fitting). Data shown are from one experiment with one (out of two) T cell donors with individual data points representing technical replicates ($n = 3$).

a

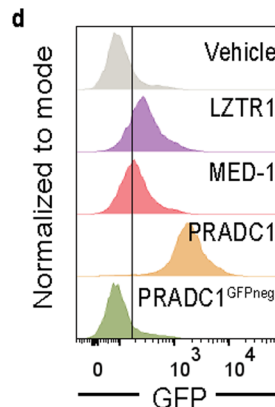


b

[AFGHILMQSTVY][ILMTV][ACDEFGHIKLMNQRSTVWY][CNST]D
[ACIMSTV][ACDFGHIMNQSTVWY]Y[ACITV]

c

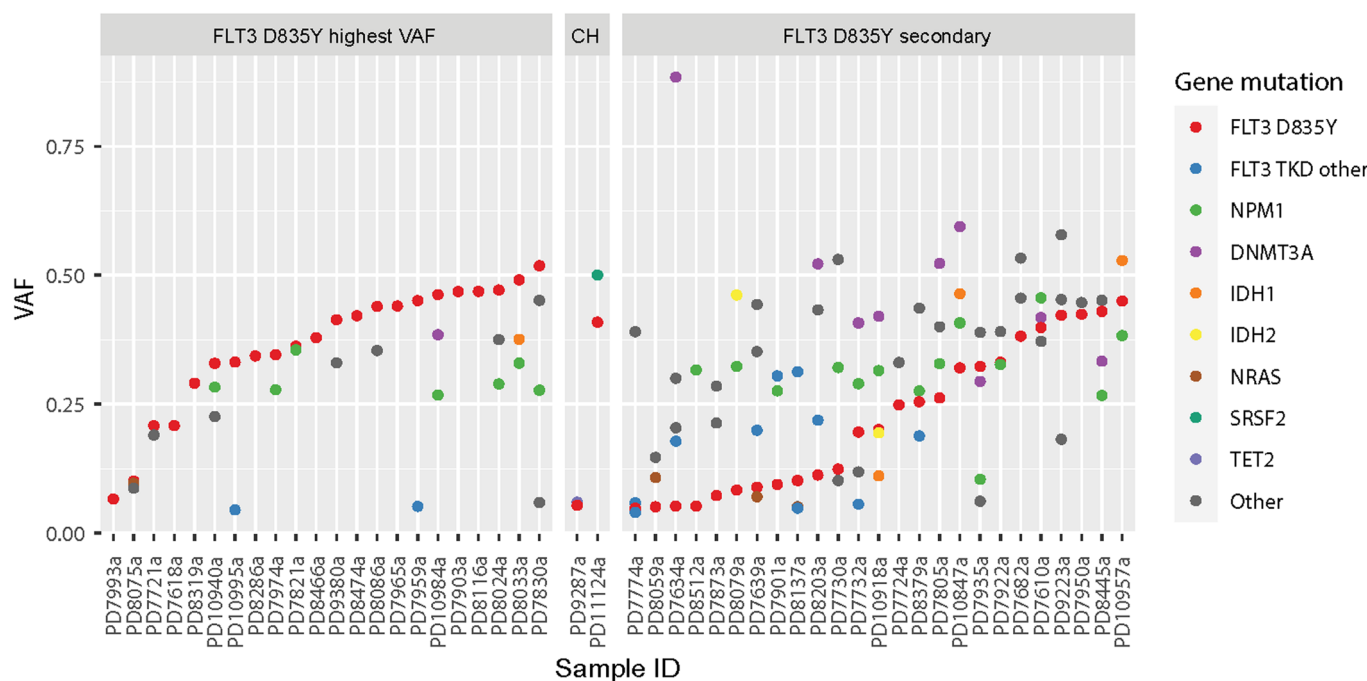
LZTR1 383-414aa: ELPSGRLFHAAAVISDAMYFGGTVDNNIRSG
MED-1 91-120aa: GSHLSASGTECYITSDMFYVEVQLDPAGQL
PRADC1 108-138aa: GGRAVIISDNADNDSFYVEMIQDSTQRTAD



Extended Data Fig. 4 | Mapping of peptide specificity does not reveal unintended targets to which the TCR^{FLT3D/Y} cells cross-react. (a) Graphs depicting IFN- γ response of TCR^{FLT3D/Y} cells to K562 cells loaded with individual peptides from mimotope library containing a total of 161 nine-mers for the FLT3^{D/Y} peptide, at a concentration of 10^{-8} M. Purple dots in each graph represent response to the FLT3^{D/Y} peptide. Substituted amino acid in the original peptide is highlighted. IFN- γ concentration range for positive reactions was 5000–35000 pg/mL (cut-off indicated by horizontal lines). Graphs show results from two independent experiments that were performed, one technical replicate

(dot) per peptide and experiment. **(b)** Peptide reactivity motifs for FLT3^{D/Y} that were queried in the ScanProsite search tool against human proteome databases. Amino acids in square brackets [] indicate alternatives that are allowed for the given position in the peptide motifs. **(c)** mRNA-encoded amino acid sequences (30-32mers) derived from the sequence of the human proteins LZTR1, MED1 and PRAD1, with the candidate cross-reactive peptide identified in the ScanProsite database underlined. **(d)** Expression of mRNA encoding LZTR1, MED1 and PRAD1 sequences following electroporation of HLA-A2^{pos} K562 cells as measured by GFP-reporter fluorescence using flow cytometry.

a

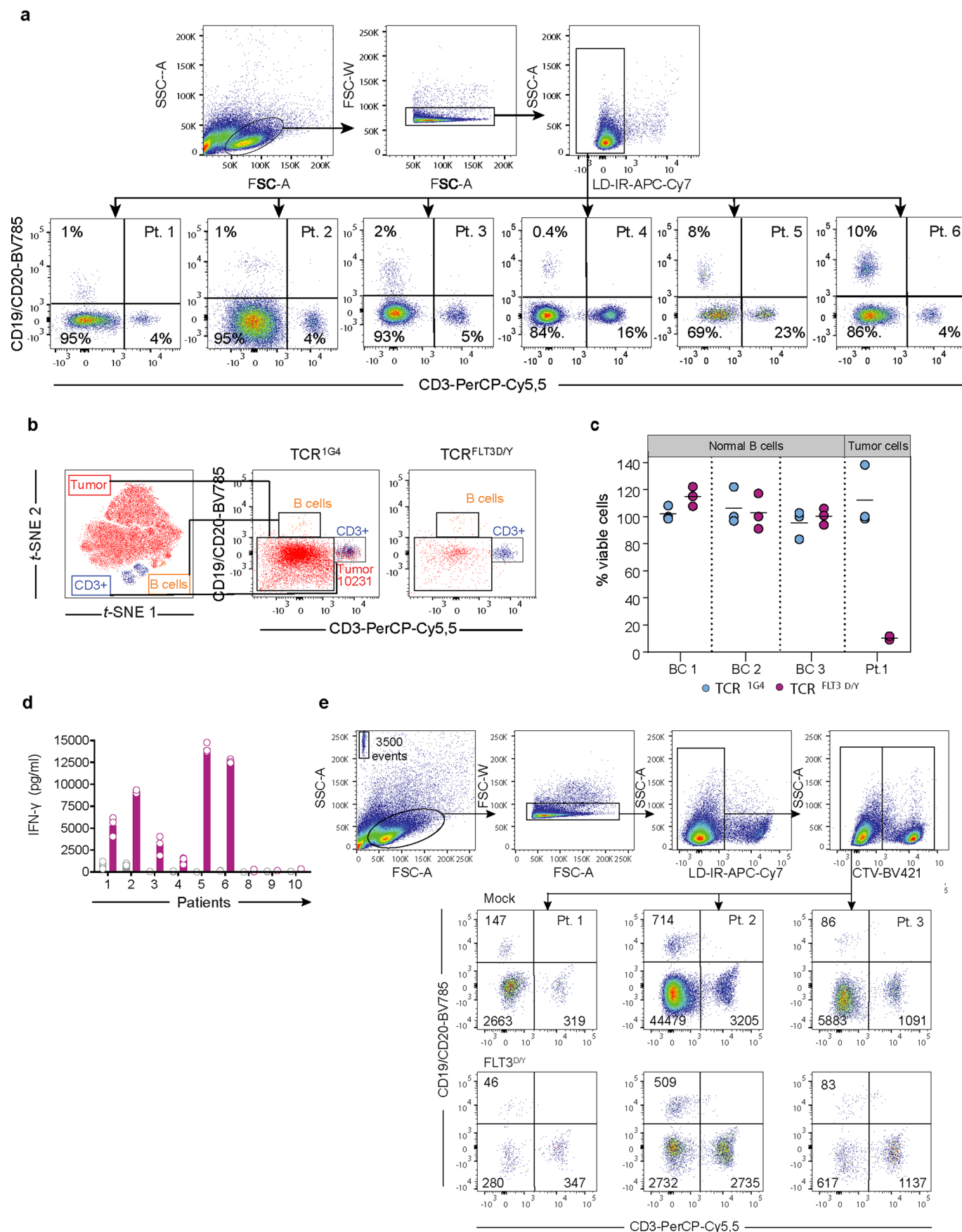


b



Extended Data Fig. 5 | Re-analysis of published mutation data for 58 FLT3 D835Y positive AML patient samples shows high VAF for FLT3 D835Y in a large fraction of patients. (a) Mutation data (SNVs and indels) from AML patients reported in Papaemmanuil *et al.*, 2016 NEJM were downloaded from <https://www.cbiportal.org/>. VAF was estimated from reported alternative allele reads divided by sequencing depth for the position. Patients harboring a FLT3 D835Y mutation were selected for in-depth analysis and displayed here. Patients are sorted from right to left within each subsection in descending order of FLT3 D835Y VAF. The following genes were considered as initiating events in clonal hematopoiesis (CH): DNMT3A, TET2, ASXL1, PPMID, JAK2, SF3B1, SRSF2, TP53,

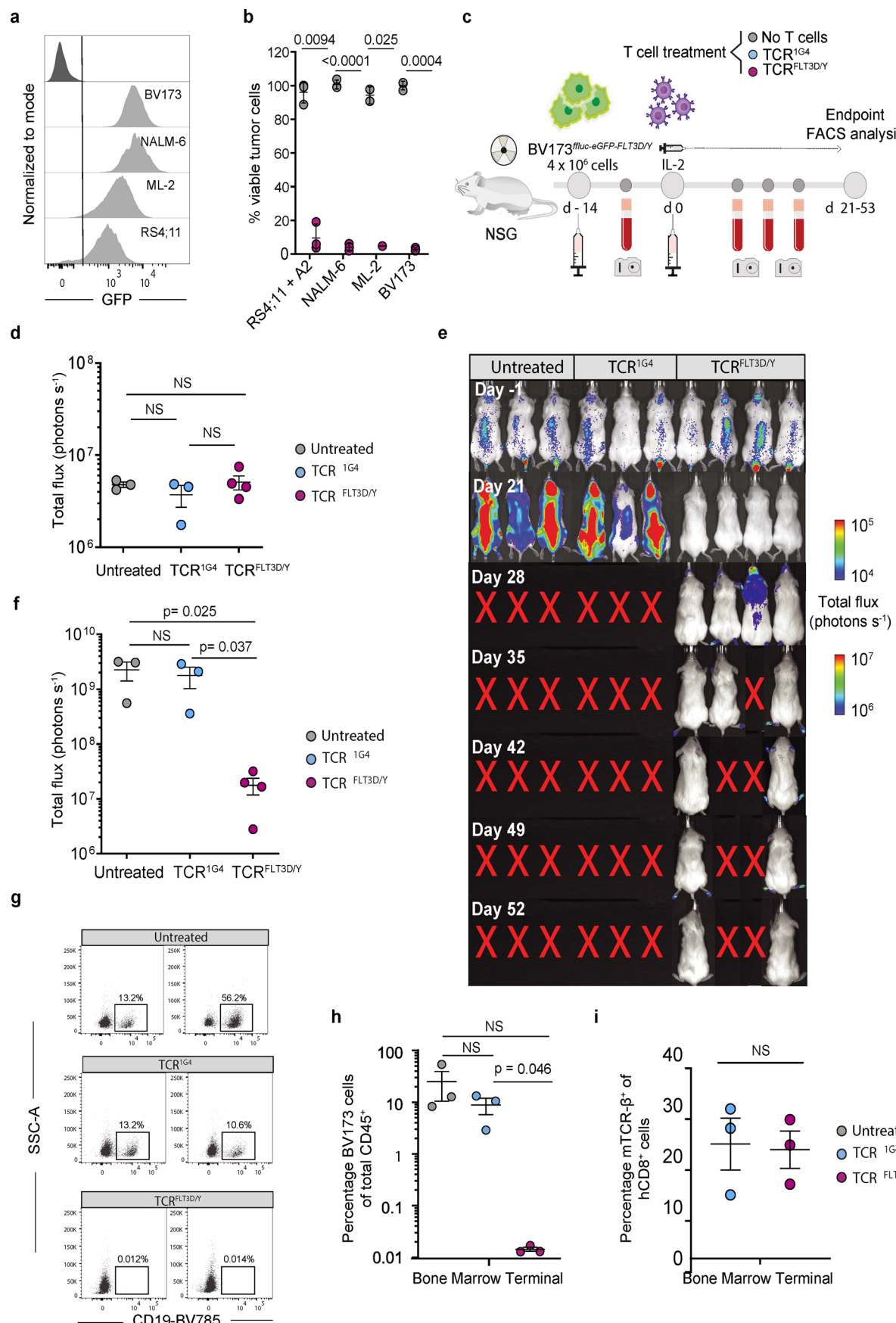
GNAS and GN1. (b) Mutation data from FLT3 D835Y positive AML patients ($n = 9$) reported in Morita *et al.*, 2020 Nat Com were downloaded. The fraction of cells with mutations (mutant cell fraction) in each AML patient with mutations are plotted in indicated colors. Patients were categorized into 3 groups; FLT3 D835Y largest, only preceded by mutations in DNMT3A, TET2, and/or ASXL1 (DTA) and/or splicing factor mutations (SF3B1, SRAF2, and U2AF1) which are closely related with clonal hematopoiesis 'CH', and the rest of cases with FLT3 D835Y mutation according to the cell fraction of mutations. Interquartile range (IQR) and median values are shown. The dashed lines indicate 1.5xIQR and the dots indicate outliers.



Extended Data Fig. 6 | See next page for caption.

Extended Data Fig. 6 | TCR^{FLT3D/Y} cells are activated by, and efficiently kill, primary AML cells expressing FLT3^{D/Y}. **(a)** Flow cytometry plots showing gating strategy to identify cell subsets in AML patient samples from PB (patient 2-6) or BM (patient 1). Cells are gated on FSC/SSC^{hi}, single, Live/Dead Fixable Near-IR events (top row), showing the fractions of CD3⁺ T cells, CD19⁺CD20⁺ B cells and myeloid cells, defined as CD3⁺CD19⁺CD20⁻ events in the bottom row. **(b)** Populations were overlaid on a t-SNE plot (patient 1) with designated colors as indicated. Inset numbers show event counts for myeloid cells after co-culture with TCR^{IG4} or TCR^{FLT3D/Y} cells, quantified as shown in e. **(c)** Quantification of normal CD19⁺ B cells isolated from $n = 3$ healthy blood donors (Buffy coat (BC) 1 - BC 3) and tumor cells from patient 1 (positive control) after performing the flow cytometry-based cytotoxicity assay for 72 h. Data points represent $n = 3$ technical replicates from one experiment and horizontal lines show mean. **(d)** Bar graph showing IFN- γ response of Mock (gray) and TCR^{FLT3D/Y} cells (purple) after 24 h

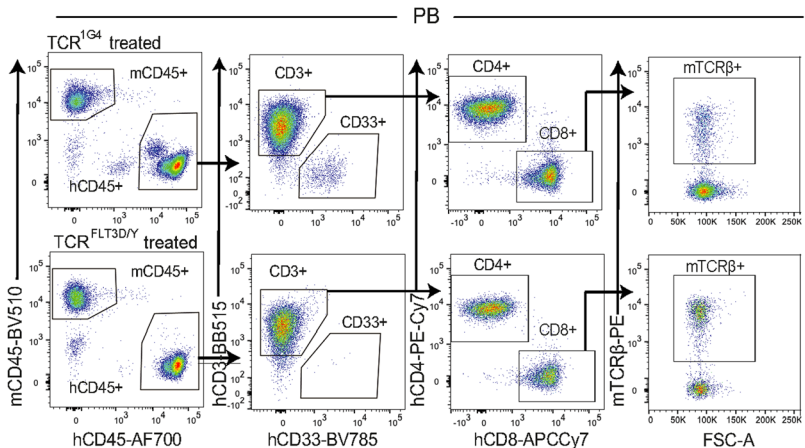
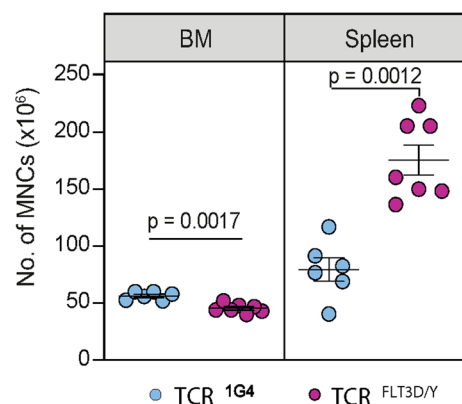
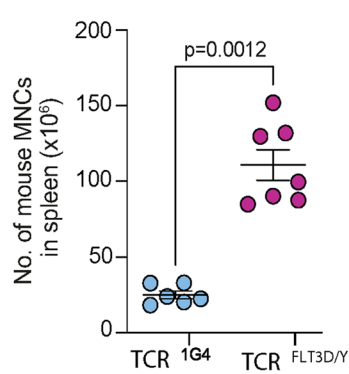
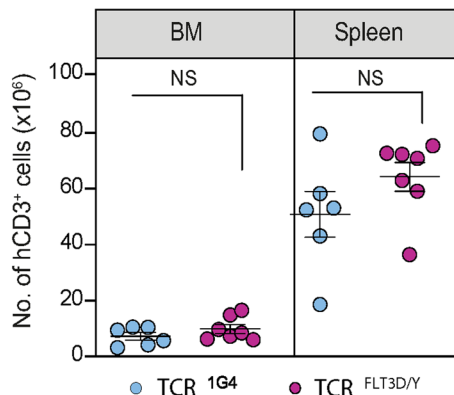
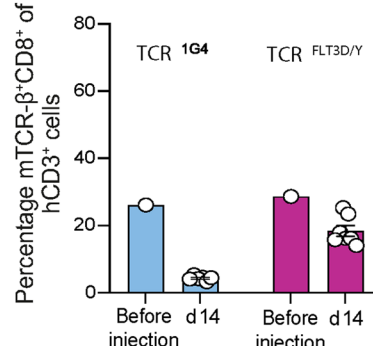
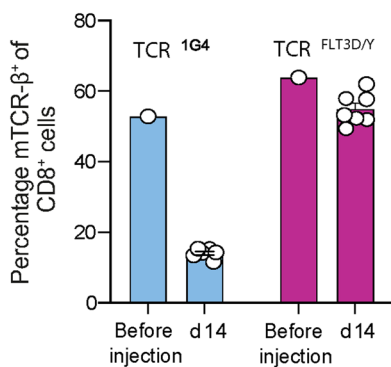
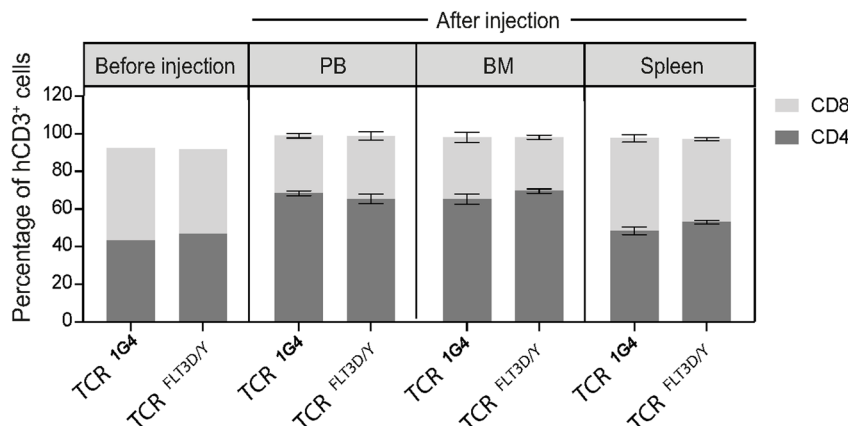
co-culture with HLA-A2^{pos} patient cells expressing the FLT3 D835Y (Pt.1-6), FLT3 D835E (Pt.9) or FLT3 D835H (Pt.10), or Pt.8 cells expressing FLT3 D835Y but being HLA-A2^{neg}. Data points represent $n = 3$ technical replicates and bars show mean. Data shown are from one experiment representative of at least two performed for each patient sample. **(e)** Gating strategy for flow cytometry cytotoxicity assay to quantify viable cells in subpopulations from AML patients 1-3 after 72 h of co-culture with autologous T cells either expressing TCR^{FLT3D/Y} (bottom row) or mock-transduced. Transduced T cells were labeled with cell-trace violet (shown in upper right plot) prior to co-culture with AML cells to distinguish them from T cells in the AML samples. Patient cell subsets are gated on FSC/SSC, singlets, Live/Dead Fixable Near-IR^{neg}, CTV^{neg} events. Numbers indicate absolute counts for CD3⁺, CD19⁺/CD20⁺ and myeloid cells after co-culture, as determined by addition of fluorescent beads (10,000) into each well and where 3,500 beads were acquired for flow cytometry analysis (shown in upper left plot).



Extended Data Fig. 7 | See next page for caption.

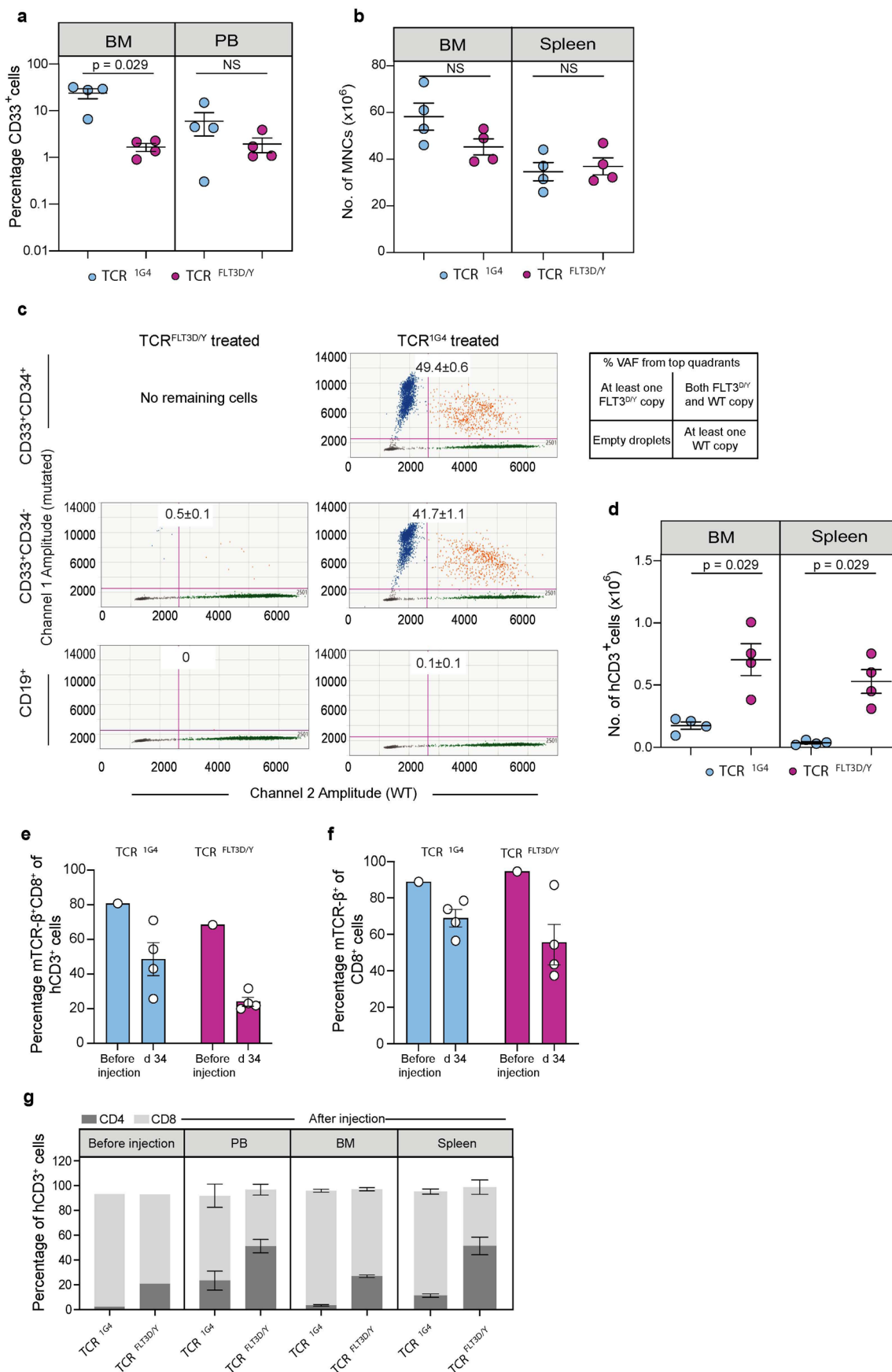
Extended Data Fig. 7 | TCR^{FLT3D/Y} cells efficiently target leukemia in a xenograft mouse model. (a) Flow cytometry histograms showing expression of FLT3^{D/Y} as measured by GFP-reporter fluorescence in transduced AML and B-ALL cell lines. Negative control (non-transduced BV173 cells) in top histogram. (b) Remaining viable FLT3^{D/Y}-transduced, HLA-A2+ cells (purple dots) after 24 h co-culture with TCR^{FLT3D/Y} cells (E:T ratio of 1:2), in percent of corresponding numbers following treatment with mock-transduced T cells (grey dots), quantified by flow cytometry. +A2 denotes that HLA-A2 was introduced by transduction. Data points are from $n = 3$ independent experiments with each dot representing the mean of $n = 3$ technical replicates in each experiment and are shown as mean \pm s.e.m. Gating strategy and quantification as shown in Extended Data Fig. 6e. (c) Schematic overview of the BV173^{D835Y} *in vivo* model. (d) Bioluminescence imaging (BLI) analysis of NSG mice day 13 after BV173^{D835Y} cell injection, one day prior to T-cell therapy. Data shown are from one experiment, with mice grouped into

untreated ($n = 3$ mice), TCR^{IG4} ($n = 3$ mice) and TCR^{FLT3D/Y} ($n = 4$ mice) cell treated. (e) BLI of BV173^{D835Y} engrafted leukemic cells in mice on indicated days relative to treatment with TCR^{IG4} or TCR^{FLT3D/Y} cells, or no treatment. (f) Quantification of BV173^{D835Y} engrafted leukemic cells in mice, 21 days after treatment with TCR^{IG4} or TCR^{FLT3D/Y} cells or left untreated. (g) Flow cytometry plots showing BM tumor burden in two untreated and two TCR^{IG4} cell-treated mice at time of sacrifice (d 21), as well as two TCR^{FLT3D/Y} cell treated mice sacrificed at end of experiment (d 53). (h) Percentage of bone marrow BV173^{D835Y} leukemic cells in mice treated with TCR^{IG4} or TCR^{FLT3D/Y} cells, or left untreated, out of total mouse and human CD45⁺ cells (21–53 days after treatment start). (i) Percentage of TCR- β^+ cells out of human CD8⁺ cells in the BM of mice analyzed at point of sacrifice. Data in d, f, h, i are presented as mean \pm s.e.m., are from one experiment with each dot representing an individual mouse, and are analyzed by unpaired, two-tailed Student's t-test. P values are shown and $p < 0.05$ was considered statistically significant.

a**b****c****d****e****f****g**

Extended Data Fig. 8 | TCR^{FLT3D/Y} cells persist *in vivo* and mediate recovery of mouse hematopoiesis in patient 7 PDX model. (a) Representative FACS plots of viable single PB MNCs from TCR^{1G4} (top) and TCR^{FLT3D/Y} (bottom) T cell-treated NSG-SGM3 mice stably engrafted with primary AML FLT3 D835Y cells from patient 7 at 14 days post T cell infusion. Equivalent gating as shown was also used for spleen. (b) Number of total MNCs in BM and spleen of TCR T cell treated mice. (c) Number of mouse MNCs (mCD45+ cells) in spleen. (d) Number of total hCD3+ cells in BM and spleen. (e-f) Percentage of mTCR-β+CD8+ cells of hCD3+ cells (e) and percentage of mTCR-β+ cells of hCD8+ cells (f) in T cell samples used for

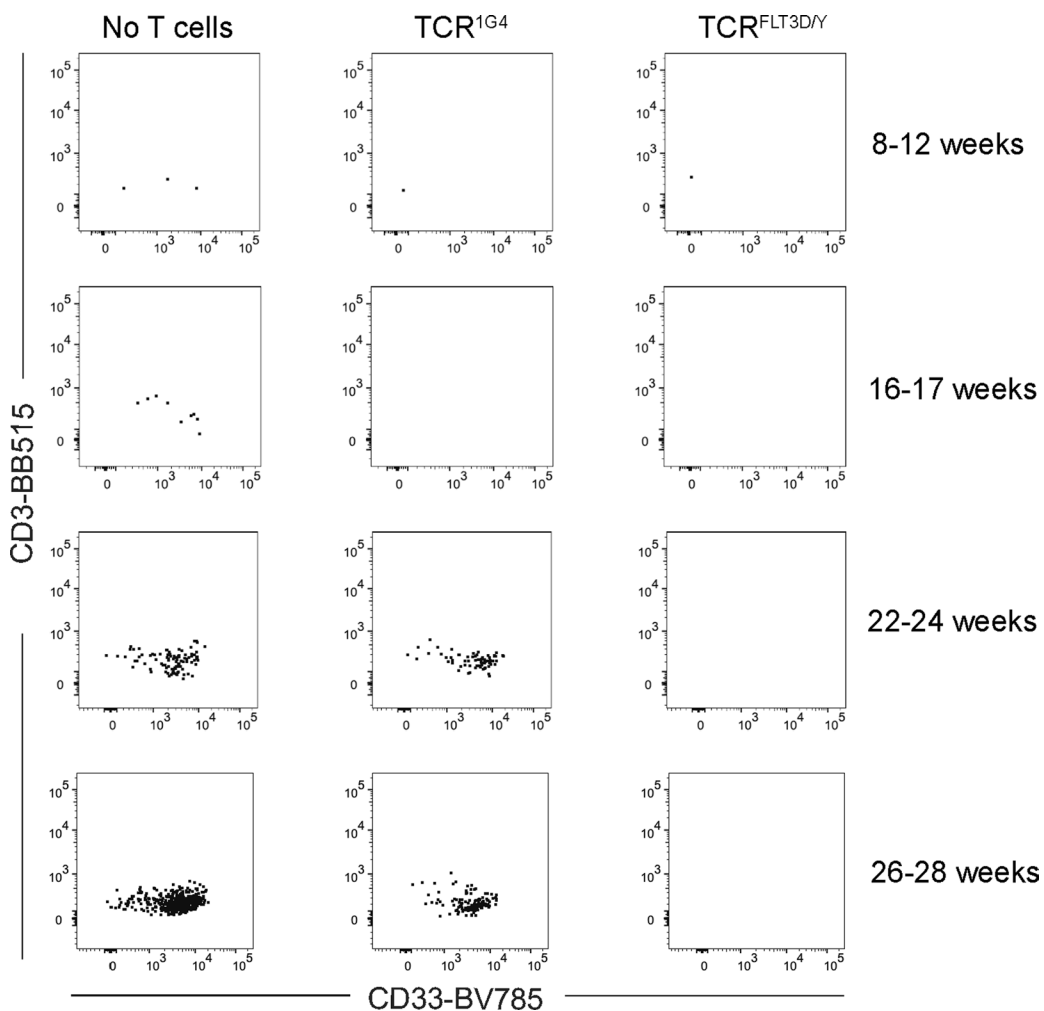
injection and at indicated days after T cell infusion, in PB. (g) Distribution (%) of CD4 and CD8 cells within the human CD3+ T cell samples used for injection, and in PB, BM and spleen 14–15 days after injection into mice. All data are from terminal analysis 15 days post T-cell infusion if not otherwise stated. The data are presented as mean ± s.e.m. of $n = 6$ individual mice treated with TCR^{1G4} cells and of $n = 7$ individual mice treated with TCR^{FLT3D/Y} cells, measured in one experiment. Each dot represents one mouse and statistical analysis was performed with two-tailed Mann-Whitney test. P values are shown and $p < 0.05$ was considered statistically significant.



Extended Data Fig. 9 | See next page for caption.

Extended Data Fig. 9 | TCR^{FLT3D/Y} cells eliminate FLT3^{D835Y} leukemia cells and persist *in vivo* in patient PDX model. (a) Percentage of CD33⁺ cells in BM and PB at endpoint (day 34 post T cell infusion) of TCR^{IG4} cell ($n = 4$) or TCR^{FLT3D/Y} cell ($n = 4$) treated mice. Numbers adjusted for hCD3⁺ T cells. (b) Number of total MNCs in BM and spleen of TCR T cell treated mice. (c) Representative ddPCR plots of BM from TCR cell-treated mice. Numbers in quadrants represent %VAF (mean \pm s.e.m.) of the FLT3^{D/Y} in BM among hCD45⁺CD33⁺CD34⁺, hCD45⁺CD33⁺CD34⁻ and hCD45⁺CD19⁺ cells from TCR^{FLT3D/Y} cell-treated (left) and TCR^{IG4} cell-treated (right) mice. ‘No remaining cells’ due to elimination of hCD45⁺CD33⁺CD34⁺ cells in TCR^{FLT3D/Y} cell-treated mice. (d) Number of total hCD3⁺ cells in BM and spleen.

(e-g) Percentage of mTCR- β^+ CD8⁺ cells of hCD3⁺ cells (e) and percentage of mTCR- β^+ cells of hCD8⁺ cells (f) in sample used for injection and at indicated days after T cell infusion in PB. (g) Distribution (%) of CD4 and CD8 cells within the human CD3⁺ T cell samples analyzed prior to injection, and in PB, BM and spleen of individual mice at endpoint. All data are from terminal analysis 34 days post T-cell infusion unless otherwise stated. The data are presented as mean \pm s.e.m. of $n = 4$ individual mice treated with TCR^{IG4} cells and of $n = 4$ mice treated with TCR^{FLT3D/Y} cells, measured in one experiment. Each dot represents one mouse and statistical analysis was performed with two-tailed Mann-Whitney test. P values are shown and $p < 0.05$ was considered statistically significant.



Extended Data Fig. 10 | Lack of *in vivo* T-cell expansion upon transplantation of primary AML cells co-cultured with TCR^{¹G⁴} or TCR^{¹LT³D/Y} T cells.

Representative FACS profiles of engrafted human CD45⁺ cells in the PB of mice analyzed at indicated weeks after transplantation of all cells remaining after

48 hours *in vitro* culture of AML cells without T cells (left), AML cells co-cultured with TCR^{¹G⁴} cells (middle) or AML cells co-cultured with TCR^{¹LT³D/Y} cells (right). Profiles are from one mouse per treatment group from one experiment out of two performed.

Reporting Summary

Nature Portfolio wishes to improve the reproducibility of the work that we publish. This form provides structure for consistency and transparency in reporting. For further information on Nature Portfolio policies, see our [Editorial Policies](#) and the [Editorial Policy Checklist](#).

Statistics

For all statistical analyses, confirm that the following items are present in the figure legend, table legend, main text, or Methods section.

n/a Confirmed

- The exact sample size (n) for each experimental group/condition, given as a discrete number and unit of measurement
- A statement on whether measurements were taken from distinct samples or whether the same sample was measured repeatedly
- The statistical test(s) used AND whether they are one- or two-sided
Only common tests should be described solely by name; describe more complex techniques in the Methods section.
- A description of all covariates tested
- A description of any assumptions or corrections, such as tests of normality and adjustment for multiple comparisons
- A full description of the statistical parameters including central tendency (e.g. means) or other basic estimates (e.g. regression coefficient) AND variation (e.g. standard deviation) or associated estimates of uncertainty (e.g. confidence intervals)
- For null hypothesis testing, the test statistic (e.g. F , t , r) with confidence intervals, effect sizes, degrees of freedom and P value noted
Give P values as exact values whenever suitable.
- For Bayesian analysis, information on the choice of priors and Markov chain Monte Carlo settings
- For hierarchical and complex designs, identification of the appropriate level for tests and full reporting of outcomes
- Estimates of effect sizes (e.g. Cohen's d , Pearson's r), indicating how they were calculated

Our web collection on [statistics for biologists](#) contains articles on many of the points above.

Software and code

Policy information about [availability of computer code](#)

Data collection

1. Flow cytometry was performed on BD LSR II Cytometer (BD Biosciences) and data was acquired with the help of BD FACSDIVA V8.0.1 software.
2. Cell sorting was performed with SH800 (Sony Biotechnology), BD FACSaria II (BD Biosciences) cell sorter and BD FACSaria Fusion cell sorter.
3. Immunoprecipitation- Mass spectrometry(IP-MS) data was acquired using an Ultimate 3000 nano-UHPLC system (Dionex, Sunnyvale, CA, USA) connected to a Q Exactive mass spectrometer (ThermoElectron, Bremen, Germany) equipped with a nano electrospray ion source.
4. Bioluminescence imaging of mice was performed with IVIS Spectrum in vivo imaging system (PerkinElmer).
5. Flow cytometry was performed on BD LSRFortessa (BD Biosciences).
6. Whole exome sequencing was performed using NextSeq.
7. Droplet digital PCR was performed using QX200 droplet generator (Bio-Rad) and QX200 droplet reader (Bio-Rad)

Data analysis

1. Flow cytometry data was analyzed with FlowJo version 9 and 10.
2. For the minigene design the peptide-MHC class I binding prediction algorithm NetMHC version 4.0 was used.
3. Numerical data was statistically analyzed and graphs were generated with the help of GraphPad Prism version 6, 7, 8 and 9 software.
4. Post-analysis of the LC-MS data was performed with Peaks DB (Bioinformatics Solutions Inc), using the Uniprot Homo sapiens database appended with the mutated protein in question.
5. Bioluminescence imaging was analyzed with Living image software version 4.5.2 (PerkinElmer)
6. Sequencing data was analyzed using the TruSight™ Myeloid Panel (Illumina, San Diego, CA, USA)
7. Curated human proteome databases UniProtKB/Swiss-Prot and Protein Data Bank were queried by employing ScanProsite tool (<https://prosite.expasy.org/scanprosite/>).
8. Whole exome sequencing reads were aligned to the human (GRCh37) genome reference using Burrows-Wheeler Aligner version 0.7.17 with default parameter settings. PCR duplicates were marked with biobambam version 2.0.87. Reads were subjected to indel realignment and

base quality score recalibration using GATK3 (version 3.8) and recalculation of MD/NM tags using SAMtools version 1.9. Mutation calling was performed through GenomonFisher (<https://github.com/Genomon-Project/GenomonFisher>). Called mutations were filtered and analyzed using R version 4.1.2.

9. Digital droplet PCR data was analyzed using QuantaSoft v1.5.38.1118 software (Bio-Rad).

For manuscripts utilizing custom algorithms or software that are central to the research but not yet described in published literature, software must be made available to editors and reviewers. We strongly encourage code deposition in a community repository (e.g. GitHub). See the Nature Portfolio [guidelines for submitting code & software](#) for further information.

Data

Policy information about [availability of data](#)

All manuscripts must include a [data availability statement](#). This statement should provide the following information, where applicable:

- Accession codes, unique identifiers, or web links for publicly available datasets
- A description of any restrictions on data availability
- For clinical datasets or third party data, please ensure that the statement adheres to our [policy](#)

The data that support the findings of this study are included in the manuscript and in supplementary information. Additional datasets used in the study are: Uniprot Homo sapiens database, using Mascot v. 2.2.07 (www.matrixscience.com) ; curated human proteome databases UniProtKB/Swiss-Prot and PDB (Protein Data Bank) by ScanProsite tool (<https://prosite.expasy.org/scanprosite/>); and peptide-MHC class I binding prediction algorithm NetMHC version 4.0 (<http://www.cbs.dtu.dk/services/NetMHC/>); data from Papaemmanuil et al NEJM 2016 (PMID: 27276561, <https://www.ncbi.nlm.nih.gov/pmc/articles/PMC5308771/>); data from Morita et al Nat Commun 2020 (PMID: 33087716). Exome sequencing data have been deposited at the European Genome-phenome Archive (EGA), which is hosted by the EBI and the CRG, under accession number EGAS00001007467. Mass spectrometry data have been deposited at the Proteomics Identification Database (PRIDE) under accession number PXD043908.

Human research participants

Policy information about [studies involving human research participants and Sex and Gender in Research](#).

Reporting on sex and gender

Information regarding the patients' sex was collected and reported in Supplementary Table 2, main manuscript. This information was not considered during the design of the study but was part of the overall clinical information obtained at the hospital. No sex or gender based analysis was performed because all data generated from each patient is shown individually in the manuscript.

Population characteristics

Information about patient, disease and sample characteristics that was collected has been shown in the manuscript (Supplementary Table 2, Supplementary Table 3)

Recruitment

Approvals from the Institutional Review Board and the Regional Committee for Medical and Health Research Ethics (REC) South-East, Norway to use primary human diagnostic blood and bone marrow samples from adult patients in the study were obtained, as were informed written consent from the patients themselves. Patient samples were selected for testing after reviewing clinical diagnostic information regarding FLT3 TKD mutation and HLA-A2 status (positive/negative). PB mononuclear cells (PBMCs) from healthy donor buffy coats were obtained from the blood bank of Oslo University Hospital, and PB or bone marrow mononuclear cells from leukemia patients were from biobanked, cryopreserved material (ethical approval numbers 2018/879, 2018/1246 and 2015/2357) or collected from Aarhus University Hospital with informed consent and ethical approval (1-45-70-88-21) and Karolinska University Hospital (2017/2085-31/2).

Ethics oversight

This study was approved by the Regional Committee for Medical and Health Research Ethics (REC) South-East Norway (2018/879, 2018/1246, and 2015/2357), the institutional Review Board and the Data Protection Officer, Oslo University Hospital, Swedish Ethical Review Authority, Stockholm (EPN 2017/2085-31/2), Ethical Committee in Central Denmark Region (1-45-70-88-21) and performed in accordance with the Declaration of Helsinki. Norwegian Food Safety Authority (application ID: 17500) and Stockholms Djurförsöketiska nämnd (17978-2018) approved all animal experiments.

Note that full information on the approval of the study protocol must also be provided in the manuscript.

Field-specific reporting

Please select the one below that is the best fit for your research. If you are not sure, read the appropriate sections before making your selection.

Life sciences

Behavioural & social sciences Ecological, evolutionary & environmental sciences

For a reference copy of the document with all sections, see nature.com/documents/nr-reporting-summary-flat.pdf

Life sciences study design

All studies must disclose on these points even when the disclosure is negative.

Sample size

In the experiment with the xenograft leukemia cell line model we expected to see 50% decrease in the tumor bioluminescence signal in the

Sample size

treated animals compared to the control T-cell treated mice. In order to reach a p value of 0.05 with 95% power, we chose to have at least 3 mice per group.

For PDX models; no calculation of sample size was used, but sample size was determined based on expected treatment efficacy following the results observed on the xenograft model, where a minimum of 4 mice were included in each treatment group. This is also in line with other studies in the field from us and others (Ali, Giannakopoulou et al Nature Biotechnology 2022 and Jain, Zhao et al Nature 2023). Apart from this lower limit of number of mice, the number of patient cells available for transplantation was determining sample size of recipient mice. In PDX model 1, 6 mice were treated with 1G4 TCR T cells and 7 mice with FLT3D/Y TCR T cells. In PDX model 2, 4 mice in each treatment group was included. One mouse was left untreated and used for whole exome sequencing. In PDX model 3, four mice in each treatment group was included. In PDX model 4, at the start of the experiment 6 mice were engrafted with FLT3D/Y TCR and 1G4 TCR AML cultures each, and 4 mice with AML cultures without T cells, but some mice were excluded from analysis (see below).

For the in vitro experiments, at least three independent experiments were generally performed with different donors/patients. If less than three experiments were performed, a rationale is normally provided in the corresponding results section or figure legend. If less than three experiments were performed, no statistical calculations are applied.

Data exclusions

For all the PDX models, only mice that were able to be followed until the end of the experiment was included. No mice were excluded for PDX cohort 1, 2 and 3. For PDX model 4, a total of 5 mice were excluded. Three mice were excluded due to uncertainties during the intra-bone injections into the mice (one FLT3D/Y TCR and two 1G4 TCR) and two mice (one 1G4 TCR and one untreated) were excluded from the analysis because they were found dead before the last peripheral blood analysis was done and could therefore not be followed for the whole experiment. In the end, that left 5 FLT3D/Y TCR treated mice, 3 1G4 TCR treated mice and 3 untreated mice for the analysis.

No mice were excluded from the leukemia cell line model.

If 50% mean difference and standard deviation 17.5%, then we require n=3 per group.

Replication

Only one experiment was performed for the xenograft mouse model. This served as a proof of principle for FLT3TCR-mediated killing of mutation-expressing cells using a cell line not naturally expressing the target FLT3D835Y, which we introduced via retroviral transduction. The efficacy observed in this model provided the rationale for further testing of the TCR-T cell therapy in four disease-relevant mouse models, where NSG mice were engrafted with patient-derived acute myeloid leukemia cells.

Two independent patients were used to establish PDX models, and effective elimination of leukemic cells were observed using both patient models. Further, one of the patients (patient 1) was used in 3 different PDX models (model 2-4) and all showed similar results, indicating reproducibility. Finally, 2 independent experiments with PDX model 4 was done, and data presented is pooled from both with n = 4 and n = 7 respectively. These mice were distributed among treatment groups as followed:

Exp nr. 1, 2 FLT3D/Y TCR treated, 1 1G4 TCR treated and 1 untreated

Exp nr 2, 3 FLT3D/Y TCR treated, 2 1G4 TCR treated and 2 untreated

For all the in vitro data at least three independent experiments were generally performed, showing successful replication of data, as described in detail in figure legends.

Randomization

In the experiment with the xenograft leukemia cell line model, mice injected with tumor were randomly assigned in different groups one day before T cell therapy. There was no difference in the tumor BLI signal between experimental groups before start of therapy (data shown in the manuscript).

For experiments using PDX model 1-3, mice mice were assigned to different treatment groups based upon their engraftment levels in blood to ensure that both groups had similar mean engraftment levels. For PDX model 2, mice were also allocated based on sex so that there were equal number of male and female mice in each treatment group. For experiments using PDX model 4, co-cultures were injected randomly into mice. For the in vitro experiments, randomization was not performed as it was not applicable and is not generally performed in the field.

Blinding

Investigators were not blinded to allocation of mice during experiments and analysis. Blinding would be impractical due to the limitations related to manpower, and because of the potential alloreactivity that needed to be closely assessed. Due to the nature of the other in vitro experiments, blinding was not possible and is not generally performed in the field as the data acquisition is quantitative (flow cytometry or MS) rather than qualitative and therefore less influenced by observer bias.

Reporting for specific materials, systems and methods

We require information from authors about some types of materials, experimental systems and methods used in many studies. Here, indicate whether each material, system or method listed is relevant to your study. If you are not sure if a list item applies to your research, read the appropriate section before selecting a response.

Materials & experimental systems

- | | |
|-------------------------------------|-------------------------------|
| n/a | Involved in the study |
| <input type="checkbox"/> | Antibodies |
| <input checked="" type="checkbox"/> | Eukaryotic cell lines |
| <input checked="" type="checkbox"/> | Palaeontology and archaeology |
| <input type="checkbox"/> | Animals and other organisms |
| <input checked="" type="checkbox"/> | Clinical data |
| <input type="checkbox"/> | Dual use research of concern |

Methods

- | | |
|-------------------------------------|------------------------|
| n/a | Involved in the study |
| <input checked="" type="checkbox"/> | ChIP-seq |
| <input type="checkbox"/> | Flow cytometry |
| <input checked="" type="checkbox"/> | MRI-based neuroimaging |

Antibodies

Antibodies used

The following fluorescently conjugated anti-human and anti-mouse antibodies were acquired from BD Biosciences or BioLegend

Antibodies used

unless otherwise specified: Anti-human CD3 (SK7, UCH-T1, HIT3a), -CD4 (OKT4, RPA-T4, SK3), -CD8a (HIT8a, RPA-T8), -CD11b (ICRF44), -CD13 (WM15), -CD14 (HCD14, M5E2), -CD16 (3G8, NKP15), -CD19 (HIB19, SJ25c1, 4G7), -CD20 (2H7), -CD33 (P67.6, VM-53), -CD34 (561, 581, 8G12), -CD38 (HB-7), -CD45 (30-F11, H130), -CD45RA (HI100), -CD45RO (UCHL1), -CD56 (NCAM, N901 Beckman Coulter), -CD57 (QA17A04), -CD62L (DREG-56), -CD123 (6H6), -CD135 (BV10A4H2), -CD137 (4B4-1), -CD197 (G043H7), -HLA-A2 (BB7.2), -HLA-DR (L243), anti-mouse CD45 (30-F11) and -Ter199 (TER119). Anti-mouse TCR- β chain (H57-597) was used to determine transduction efficiency of the TCR1G4 or TCRFLT3D/Y in human cells and monitor transduced T cells used for in vivo treatment in mice. Live/Dead Fixable Near-IR Dead Cell Stain kit and Aqua Dead Cell Stain kit (Life Technologies), 7AAD (Sigma Aldrich) or DAPI (ThermoFisher) was used to exclude dead cells in all flow cytometry experiments. The following antibodies for ELISA were acquired from BD Pharmingen or R&D systems: mouse anti-human IFN γ capture antibody (NIB42) and Biotin Mouse Anti-Human IFN γ detection antibody (4S.B3). Detailed information is provided in Supplementary Table 10 and below:

CD3 PerCP-Cy5.5, APC-Cy7, BB515, SK7, UCH-T1, HIT3a Mouse, anti-human Biolegend, Biolegend, BD 344808, 300426, 565100 1:200, 1:200, 1:100-1:200 Flow cytometry (BB515) 7158825/
9021562/
9205788/
0077790

CD4 BUV395, PE-Cy5, BV711 RPA-T4, OKT4 Mouse, anti-human BD, Biolegend, Biolegend 564724, 300512, 317440 1:300, 1:300, 1:200 Flow cytometry (BUV395) 35962, (PE-Cy7) B269744/
B288879

CD8a AF700, BV421, APC-Cy7 HIT8a, RPA-T8 Mouse, anti-human Biolegend 300920, 301036, 301016 1:200, 1:200, 1:80-1:300 Flow cytometry (APC-Cy7) B274260/B300873

CD11b FITC ICRF44 Mouse, anti-human Biolegend 301330 1:200 Flow cytometry

CD13 BV711 WM15 Mouse, anti-human Biolegend 301722 1:200 Flow cytometry

CD14 FITC, BV711, PE-Cy7 HCD14, M5E2 Mouse, anti-human Biolegend 325604, 301838, 301820 1:200 Flow cytometry

CD16 FITC 3G8, NKP15 Mouse, anti-human Biolegend, BD 302006, 335035 1:200, 1:100 Flow cytometry

CD19 BV785, BV421, FITC HIB19, SJ25c1, 4G7), Mouse, anti-human Biolegend, Biolegend, BD 302240, 363018, 345776 1:200, 1:200-1:300, 1:100 Flow cytometry (BV421) B237452/B313190

CD20 BV785 2H7 Mouse, anti-human Biolegend 302356 1:200 Flow cytometry

CD33 APC-Cy7, BV785 P67.6, VM-53 Mouse, anti-human Biolegend 366614, 303428 1:200 Flow cytometry (BV785) B252804/
B260381/
B297609

CD34 BV785, AF647, APC 561, 581, 8G12 Mouse, anti-human Biolegend, Biolegend, BD 343626, 343508, 345804 1:200 Flow cytometry (APC) 7348707

CD38 PE-Cy7 HB-7 Mouse, anti-human Biolegend 356608 1:200 Flow cytometry

CD45 BV605, AF700 H130 Mouse, anti-human Biolegend 304042, 304024 1:200, 1:200-1:600 Flow cytometry (AF700) B284831/
B306873

CD45 BV510 30-F11 Rat, anti-mouse Biolegend 103138 1:400-1:800 Flow cytometry B251556/
B305756

CD45RA PE HI100 Mouse, anti-human BD 555489 1:100 Flow cytometry

CD45RO APC UCHL1 Mouse, anti-human BD 340438 1:100 Flow cytometry

CD56 BV650, ECD NCAM, N901 Mouse, anti-human BD, Beckman Coulter 564057, A82943 1:200 Flow cytometry

CD57 BV605 QA17A04 Mouse, anti-human Biolegend 393303 1:200 Flow cytometry

CD62L PE-Cy7 DREG-56 Mouse, anti-human Biolegend 304822 1:200 Flow cytometry

CD123 BV605 6H6 Mouse, anti-human Biolegend 306026 1:200 Flow cytometry

CD135 PerCP-Cy5.5 BV10A4H2 Mouse, anti-human Biolegend 313316 1:200 Flow cytometry

CD137 PE 4B4-1 Mouse, anti-human BD 555956 1:20 Flow cytometry

CD197 (CCR7) FITC G043H7 Mouse, anti-human BioLegend 353216 1:100 Flow cytometry

HLA-A2 PE, BV650 BB7.2 Mouse, anti-human BioLegend 343305, 343306, 343324 1:100, 1:200 Flow cytometry (PE) B279657 (BV650) B290341

HLA-DR AF700 L243 Mouse, anti-human BioLegend 307626 1:200 Flow cytometry

TCR β PE H57-597 Mouse, anti-human BioLegend 109208 1:200 Flow cytometry B219253

Ter119 PE-Cy5, BUV395 TER-119 Mouse, anti-human Biolegend, BD 116210, 566206 1:600, 1:200 Flow cytometry (PE-Cy5) B208715/B277009 (BUV395) 7235927

7AAD Biolegend 1:200 Flow cytometry 126M4105V

DAPI Invitrogen 1:50000 Flow cytometry 184346

LIVE/DEAD™ Fixable Near-IR Thermo Fisher Scientific L10119 1:1000 Flow cytometry

LIVE/DEAD™ Fixable Aqua Dead Cell Stain Kit Thermo Fisher Scientific L34957 1:200 Flow cytometry

Cell Trace Violet Thermo Fisher Scientific C34557 1:3300 Flow cytometry

5-(and-6)-Carboxyfluorescein Diacetate, Succinimidyl Ester Thermo Fisher Scientific C1157 1:2000 Flow cytometry

Streptavidin PE, APC Thermo Fisher Scientific S866, S868 Flow cytometry

Purified Mouse Anti-Human IFN- γ NIB42 BD 551221 1:500 ELISA

Biotin Mouse Anti-Human IFN- γ 4S.B3 BD 554550 1:500 ELISA

Validation

All antibodies used in the study are available commercially and have been validated by commercial vendors for use in research or diagnostics. Furthermore, all antibodies used have been individually titrated prior to use to identify their optimal concentration in the required application. Detailed information is provided in Supplementary Table 10.

Eukaryotic cell lines

Policy information about [cell lines and Sex and Gender in Research](#)

Cell line source(s)

The following cell lines were all authenticated and obtained from American Type Culture Collection (ATCC) or German Collection of Microorganisms and Cell Cultures (DSMZ) or were kindly gifted (giver in parenthesis): NALM-6 and BV173 (Dr.

June Myklebust), RS4;11 (DSMZ), T2 (ATCC), RD (ATCC), U-2 OS, U-87 MG, ML-2, FM6 and COLO 668 (Dr. Fridtjof Lund-Johansen), UT-7 (DSMZ), HeLa (Dr. Andreas Brech), HaCaT (Dr. Frode Jahnsen), MCF7 (Dr. Matthias Leisegang), K562 (ATCC), EA.hy926 (ATCC), Daoy (ATCC), HCT-116 (DSMZ), CHP-212 (DSMZ), OCI-M2 (DSMZ), HEK 293 (ATCC), Hep G2 (ATCC), MV-4-11 (DSMZ), EoL-1 (DSMZ), MOLM-13 (DSMZ), Caco-2 (Dr. Ragnhild A. Lothe), HEL 92.1.7 (ATCC), HLA class-I deficient B721.221 cells were obtained from FRED HUTCH Research Cell Bank, UT-7, Phoenix-AMPHO (ATCC). EBV-LCL cell line was previously generated in-house by immortalizing human PBMC's from HLA-A2 positive and negative donors with Epstein-Barr viral supernatants. Sex or gender of the origin of cell lines was not taken into consideration and cell lines were selected based on HLA and tissue origin. All cell lines were cryopreserved in aliquots labeled according to passage and only low passage cell lines were used to start fresh cultures

Authentication

Authenticated cell lines (STR DNA profiling) were purchased from ATCC or DSMZ: RS4;11, T2, RD, K562, EA.hy926, Daoy, HCT-116, CHP-212, HEL, 92.1.7, B721.221, MV4-11, EoL-1, MOLM-13, Phoenix AMPHO, and cryopreserved aliquots labeled according to passage. Only low passages (1-4 passages) were used to start cultures. The identity of the passage used (5 or higher) experimentally of the cell lines NALM-6, BV173, U-2 OS, FM6, HeLa, HaCaT, MCF7, COLO 668, U-87MG , ML-2, OCI-M2, HEK 293, Caco-2, UT-7, Hep G2 was ascertained by short tandem repeat DNA profiling, a service provided by Labcorp DNA identification LAB, NC, USA (formerly Genetica, <https://celllineauthentication.com/>). In-house immortalized EBV-LCL cells were regularly tested for CD20 or CD19 staining to confirm their B cell origin.

Mycoplasma contamination

Cells were tested regularly for mycoplasma contamination and were confirmed negative before experimental use

Commonly misidentified lines (See [ICLAC](#) register)

No commonly misidentified cell lines were used in the study.

Animals and other research organisms

Policy information about [studies involving animals](#); [ARRIVE guidelines](#) recommended for reporting animal research, and [Sex and Gender in Research](#)

Laboratory animals

In PDX model 1, NSG-SGM3 mice (NOD.Cg-Prkdcscid Il2rgtm1Wjl Tg(CMV-IL3,CSF2,KITLG)1Eav/MloySzJ) stably engrafted with primary FLT3D/Y HLA-A2pos AML patient cells at 5 weeks of age were obtained from the Jackson Laboratory (Stock ID J000106565). In PDX model 2, NSG-SGM3 mice (NOD.Cg-Prkdcscid Il2rgtm1Wjl Tg(CMV-IL3,CSF2,KITLG)1Eav/MloySzJ), obtained from Jackson Laboratory; stock 013062) were engrafted with FLT3D/Y HLA-A2pos AML patient cells at 9 weeks of age. In PDX model 3, NSG mice (NOD.Cg-Prkdcscid Il2rgtm1Wjl/SzJ, obtained from Jackson Laboratory; stock 005557) were engrafted at 12-13 weeks of age with FLT3D/Y HLA-A2pos AML patient cells previously engrafted into NSG mice at 8-13 weeks of age. In PDX model 4, NOG-hIL2 mice (NOD.Cg-Prkdcscid Il2rgtm1Sug Tg(CMV-IL2)4-2Jic/JicTac, obtained from Taconic) engrafted with FLT3D/Y HLA-A2pos AML patient cells at 14 weeks of age were used as donors for co-cultures. Co-cultures were transplanted into NSG mice (NOD.Cg-Prkdcscid Il2rgtm1Wjl/SzJ, obtained from Jackson Laboratory; stock 005557) at 8-13 weeks of age. All mice were housed 2-5 mice per cage in IVC-Mouse GM 500 cages with a light cycle of 4 a.m – 4 p.m (patient 7) or 6 a.m – 6 p.m (patient 1), 21°C and 50% humidity. The maximal tumour burden permitted by the ethics committee/institutional review board was defined by the impact on the animal's health. Briefly, mice engrafted with leukemic cells were continuously monitored for signs of poor health according to Oslo University's and Karolinska Institutet's health assessment where animals receiving a score above 0.4 points were terminated. In our experiments, no animal exceeded the humane endpoint. For establishing xenograft leukemia cell line model, 8- to 10-weeks-old female NOD.Cg-Prkdcscid Il2rgtm1Wjl/SzJ (nsg) mice were used. All mice were housed 6 mice per cage in Eurostandard type III cages (macrolone) with a light cycle of 7 a.m – 7 p.m, 22 ± 1C and 62 ± 5% humidity. Maximum tumor burden for leukemia is indirectly measured. Mice were observed for clinical signs of tumor spread and were sacrificed if they developed >20% weight loss, hunched posture, ruffled fur, limb paralysis or enlarged spleens (distended abdomens, enlarged and palpable spleens). Maximum tumor burden was not exceeded. Experiments were terminated 2 months after T-cell injection to avoid graft-versus-host disease, and surviving mice in treated groups were humanely sacrificed.

Wild animals

No wild animals were used.

Reporting on sex

For the xenograft leukemia cell line model only female mice were used. In PDX model 2, both male and female mice were used and equally distributed between the treatment groups. For all other PDX models, only female mice were used.

Field-collected samples

No field-collected samples were used.

Ethics oversight

Experiments were performed according to the guidelines and obtained permissions from the ethics committees at Stockholm Norra Djurförsökssetiks Nämd (17978-2018) and Norwegian Food Safety Authority (17500). For the cell line xenograft model, mice were observed for clinical signs of tumor spread and were sacrificed if they developed >20% weight loss, hunched posture, ruffled fur, limb paralysis or enlarged spleens (distended abdomens, enlarged and palpable spleens). Experiments were terminated 2 months after T-cell injection to avoid graft-versus-host disease, and surviving mice in treated groups were humanely sacrificed. The maximum tumor burden was not exceeded in any mice. For the PDX models the maximal tumour burden permitted was defined by the impact on the animal's health. Briefly, mice engrafted with leukemic cells were continuously monitored for signs of poor health according Karolinska Institutet's health assessment where animals receiving a score above 0.4 points were terminated. In our experiments, no animal exceeded the humane endpoint.

Note that full information on the approval of the study protocol must also be provided in the manuscript.

Dual use research of concern

Policy information about [dual use research of concern](#)

Hazards

Could the accidental, deliberate or reckless misuse of agents or technologies generated in the work, or the application of information presented in the manuscript, pose a threat to:

- | | |
|-------------------------------------|---|
| No | Yes |
| <input checked="" type="checkbox"/> | <input type="checkbox"/> Public health |
| <input checked="" type="checkbox"/> | <input type="checkbox"/> National security |
| <input checked="" type="checkbox"/> | <input type="checkbox"/> Crops and/or livestock |
| <input checked="" type="checkbox"/> | <input type="checkbox"/> Ecosystems |
| <input checked="" type="checkbox"/> | <input type="checkbox"/> Any other significant area |

Experiments of concern

Does the work involve any of these experiments of concern:

- | | |
|-------------------------------------|--|
| No | Yes |
| <input checked="" type="checkbox"/> | <input type="checkbox"/> Demonstrate how to render a vaccine ineffective |
| <input checked="" type="checkbox"/> | <input type="checkbox"/> Confer resistance to therapeutically useful antibiotics or antiviral agents |
| <input checked="" type="checkbox"/> | <input type="checkbox"/> Enhance the virulence of a pathogen or render a nonpathogen virulent |
| <input checked="" type="checkbox"/> | <input type="checkbox"/> Increase transmissibility of a pathogen |
| <input checked="" type="checkbox"/> | <input type="checkbox"/> Alter the host range of a pathogen |
| <input checked="" type="checkbox"/> | <input type="checkbox"/> Enable evasion of diagnostic/detection modalities |
| <input checked="" type="checkbox"/> | <input type="checkbox"/> Enable the weaponization of a biological agent or toxin |
| <input checked="" type="checkbox"/> | <input type="checkbox"/> Any other potentially harmful combination of experiments and agents |

Flow Cytometry

Plots

Confirm that:

- The axis labels state the marker and fluorochrome used (e.g. CD4-FITC).
- The axis scales are clearly visible. Include numbers along axes only for bottom left plot of group (a 'group' is an analysis of identical markers).
- All plots are contour plots with outliers or pseudocolor plots.
- A numerical value for number of cells or percentage (with statistics) is provided.

Methodology

Sample preparation

Samples analyzed by flow cytometry contained mononuclear cells in suspension isolated from buffy coats by lymphoprep density gradient centrifugation that were cultured with standard media as detailed in the manuscript. Patient blood or bone marrow samples were harvested for diagnostic purposes and mononuclear cells were isolated by lymphoprep density gradient centrifugation. Samples were then cryopreserved and stored in liquid nitrogen in designated cell biobanks in our institutions before use in the experiments as detailed in the methods. Cell lines utilized were cultured for variable amounts of time in recommended media before test in the experiments.

Blood samples and bone marrow were harvested from murine xenograft leukemia cell line models. RBC lysis was performed by ACK lysis buffer, followed by washing and surface or intracellular staining with different anti-bodies for flow cytometry analysis.

For the PDX mice, peripheral blood (tail vein or cardiac puncture) was harvested and processed with 1:1 Dextran followed by red blood cell lysis with ammonium-chloride and processed into single cell suspension in PBS supplemented with 1-5 % fetal calf serum and 2mM EDTA. Bone marrow (tibia, femur, crista from both hind legs) from PDX mice was harvested from PDX mice and crushed with mortar and pestle and processed into single cell suspension in PBS supplemented with 1-5 % fetal calf serum and 2mM EDTA. Spleen was processed into single cell suspension in PBS supplemented with 1-5 % fetal calf serum and 2mM EDTA. All samples were included with both anti mouse and anti human FcR-block before staining with monoclonal antibodies.

Instrument

BD LSR II (BD Biosciences) equipped with high throughput sampler (HTS), BD LRSFortessa (BD Biosciences). Cell sorting was performed with SH800 (Sony Biotechnology), BD FACSAria II (BD Biosciences) cell sorter and BD FACSAria Fusion.

Software

For data collection for all experiments, BD FACSDiva V8.0.1 was used. For data analysis FlowJo version 9 and 10 was used.

Cell population abundance

Tumor cell lines that were transduced to express the FLT3 D835Y mutation and GFP and firefly luciferase were purified by FACS with a purity > 95%.
For the PDX models purity sorts were done with >95 % purity of relevant populations. Purity was determined by sorting of >100 cells for each relevant population and re-analysis of the sorted cells.

Gating strategy

For all flow cytometry experiments FSC-A/SSC-A was used for gating mononuclear cells. Doublets were excluded. 7AAD, DAPI Live/dead fixable near-IR -or Live/dead Aqua positive cells were gated out to exclude non-viable cells.

For pMHC multimer staining: From the live cell gate, CD8+ events were gated and subsequently, pMHC multimer+ events were identified as double positive for PE and APC conjugated pMHC multimers.

For flow cytometry based cytotoxicity assays and T cell activation assays, tumor cell lines and transduced T cells were stained with surface anti-bodies and were gated as detailed in the methods and extended data supplement. Primary patient samples were also stained with surface antibodies for the presence of CD3- CD19- CD20- myeloid cells. In this case, effector cells in the same co-culture well were pre-labeled with CellTrace Violet (CTV, Life Technologies) to distinguish from live target cells. Myeloid cells (CD3- CD19- CD20-), mature B and T cells, and CD34+lin- cells were gated and overlaid to be visualized as T-Distributed Stochastic Neighbor Embedding (tSNE) plots. CountBright Absolute Counting Beads were utilized to acquire equal numbers of events in each tested well.

To analyze presence of transduced T cells in blood and bone marrow of the xenograft leukemia cell line model, single live cells are gated as described above. Total leukocytes were defined as antigen positive for both human and mouse CD45. From CD45+ gate, human TCR transduced T cells were identified as anti-human CD3+, CD8+ and anti-mouse TCR-β+. A murine constant part was introduced into the TCR-β chain to serve as a reporter for TCR transduction.

To determine leukemic burden in PDX mice, viable (7AAD or DAPI negative) single (SSC-W vs SS-H) human and mouse leukocytes were separated based on mTer119- cells staining positive for either mouse or human CD45. Further, AML cells were determined as hCD45+CD3-CD19-CD33+. For PDX model 2, two distinct CD33+ populations were identified as CD34+ or CD34-. To track the infused T cells, the hCD45+CD3+ cells were further gated on CD4+ or CD8a+ and mTCRb+.

Tick this box to confirm that a figure exemplifying the gating strategy is provided in the Supplementary Information.